ACS OMEGA

Article

Cite This: ACS Omega 2019, 4, 4871−4887

http://pubs.acs.org/journal/acsodf

Physicochemical Properties Govern the Activity of Potent Antiviral Flavones

Xavier Martin-Benlloch,[†] Sibylle Haid,[‡] Alexandra Novodomska,[†] Frank Rominger,[§] Thomas Pietschmann,[‡] Elisabeth Davioud-Charvet,*[,†] and Mourad Elhabiri*[,†]

[†]Université de Strasbourg, Université de Haute-Alsace, CNRS, LIMA, UMR 7042, Equipe Chimie Bioorganique et Médicinale, ECPM, 25 Rue Becquerel, 67000 Strasbourg, France

[‡]Institute of Experimental Virology, TWINCORE Centre for Experimental and Clinical Infection Research; A Joint Venture of the Medical School Hannover (MHH) and the Helmholtz Centre for Infection Research (HZI), Feodor-Lynen-Str. 7, 30625 Hannover, Germany

[§]Organisch-Chemisches Institut, Ruprecht-Karls-Universität Heidelberg, Im Neuenheimer Feld 270, 69120 Heidelberg, Germany

Supporting Information

ABSTRACT: Ladanein (i.e., 5,6,7-trihydroxylated flavone) was demonstrated to act as a powerful virucidal agent toward a broad range of enveloped virus particles. Fe(III) coordination and pH are indeed among the key parameters that might favor both bioactivation of the flavone and consequent host cell entry inhibition. In this present work, the impact of fluorinated groups on the physicochemical and antiviral properties of the flavone was investigated, thus allowing a deeper understanding of the antiviral mode of action. The improved synthesis of ladanein allowed accessing a broad range of analogues, some of them being significantly more active than the former ladanein lead compound. We first determined the acido-basic properties of this homogenous series of compounds and then investigated their electrochemical behavior. Fe(III) coordination properties (stability, spectral behavior, and kinetics) of ladanein and its analogues were then examined (quasiphysiological conditions) and provided key information of their stability and reactivity. Using the determined physicochemical parameters, the critical impact of the iron complexation and medium acidity was confirmed on hepatitis C virus (HCV) particles (pre)treated with ladanein. Finally, a preliminary structure−HCV entry inhibition relationship study evidenced the superior antiviral activity of the ladanein analogues bearing an electron-withdrawing group in para position (**FCF_3** > **$FOCF_3$** > **$FFCF_3$** > **FF** > **FOMe**) on the B cycle in comparison with the parent ladanein itself.

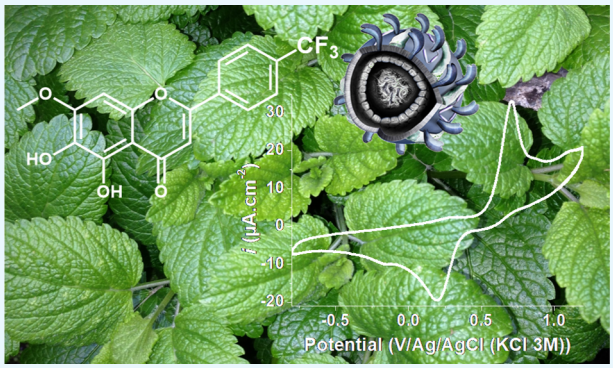

INTRODUCTION

Hepatitis C virus (HCV) is among the most significant and widespread viral diseases that affects nearly 71 million people worldwide, of whom around 50−80% will suffer chronic hepatitis that may lead to hepatocellular carcinoma and ultimately to death. During the last years, research in anti-HCV drugs has impressively increased, leading to approval of new drugs that enhance the sustained virologic response rates to greater than 95% across all clinically relevant viral genotypes. However, these drugs are in use for only a short period of time and it is therefore difficult to predict if and to what extent viral resistance will necessitate salvage therapies with alternative mode of action (MoA). Furthermore, the new therapies are expensive, thus limiting access to therapy in resource-poor areas of the world. Therefore, there is still a need for evaluation and development of alternative and/or complementary treatment strategies. These compounds may be combined to other well-known drugs to reach an all-oral therapy or treat complications arising from liver transplantation, for which current therapies are still not convenient.

Flavonoids including flavones produced by nutritive plants were shaped by evolution by enhancing both animal and human health, playing pleiotropic effects, and showing low capability to induce drug resistance.[1] A preparative bioactivity-guided fractionation approach allowed identifying a novel antiviral lead, the flavone ladanein (Figure 1) that displays an unusual 5,6,7-trihydroxylated substitution pattern on its cycle A. Ladanein was then prepared through a scalable and versatile synthetic route, and its peculiar antiviral properties were confirmed.[2,3] On the other hand, mechanistic investigations showed that ladanein exposure of lipid-enveloped HCV virions prevented the infection in a postattachment entry step. By contrast, ladanein exposure of surface-bound virions or cellular

Received: November 29, 2018
Accepted: February 19, 2019
Published: March 5, 2019

DOI: 10.1021/acsomega.8b03332
ACS Omega 2019, 4, 4871−4887

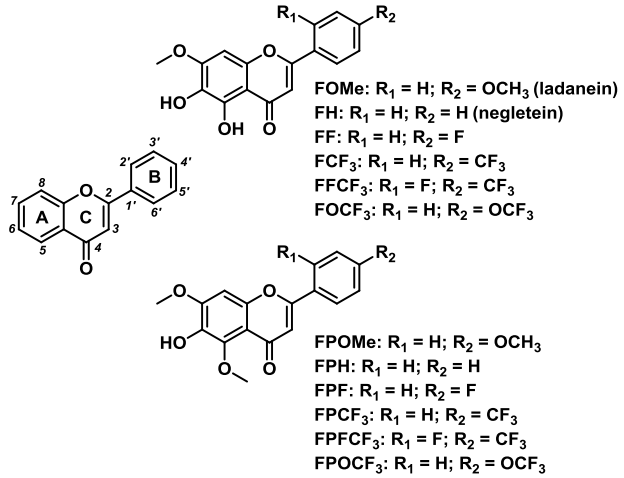

Figure 1. Chemical structures of the synthetic 6-hydroxylated flavones.

targets had a reduced or even almost no antiviral effect. Ladanein was demonstrated to act on all major HCV genotypes, including a variant that is resistant to a reference entry inhibitor.[4] Concomitantly, the active natural ladanein-enriched fractions were shown to contain high Cu and Fe levels that suggested that the virucidal activity of ladanein (i.e., Fe(III)- and pH-related bioactivation)[4] is intimately linked to its physicochemical properties (i.e., acid−base, redox, and metal complexation).[5] The former synthesis of ladanein was significantly improved and allowed preparing multigram amount of the flavone.[6] This present work was focused on the synthesis and investigation of the physicochemical properties (i.e., spectroscopy, protonation, electrochemistry, Fe(III) complexation, and formation kinetics) of six new synthetic ladanein analogues (negletein and fluorinated derivatives, Figure 1, see the Supporting Information for the characterization of the new ladanein analogues). Particular attention was paid on the impact of the introduction of fluorinated groups to the flavone core on the physicochemical and antiviral properties, allowing a much deeper understanding of the MoA of these promising antiviral compounds.

RESULTS AND DISCUSSION

Structural Properties. In this section, the X-ray structural data obtained for ladanein **FOMe** and its final precursor **FPOMe** will be discussed with respect to closely related flavones (see Figure S1 and Table 1). To the best of our knowledge, these X-ray data are the scarce ones available for this class of compounds (i.e., displaying a 5,6,7-trisubstitution on cycle A). The differences in packing of the two solid-state structures of ladanein originate mainly from a methanol molecule present in the crystal lattice, which cocrystallizes with synthetic ladanein and interacts with the 5- and 6-OH groups through hydrogen bonds (Figure 2).

For flavones containing a 4′-methoxy substituent, mesomeric effects from the OCH_3 donor to the 4-carbonyl acceptor unit (Scheme 1) likely account for the small torsion angle ($O_1-C_2-C_{1'}-C_{2'}$) measured between the B ring and the coplanar A−C benzopyran moiety (Table 1).

The $C_2-C_{1'}$ bond distances range from 1.46 Å for synthetic ladanein to 1.48 Å for 5,7,3′-trihydroxy-6,4′,5′-trimethoxy-flavone, in agreement with an sp^2-sp^2 σ bond (i.e., a length of 1.48 Å is expected for $C_{sp^2}-C_{sp^2}$ bond). The C_2-C_3 bond lengths were found to be slightly longer than a pure double bond due to conjugation (i.e., a bond length of 1.34 Å is expected for a pure double bond), similar to the C_4-O_4 bond lengths that are increased (e.g., baicalein, salvigenin, ladanein, and eupatorin) compared with flavones having a larger dihedral angle (i.e., a length of 1.22 Å is expected for a C═O double bond).[14] These structural features can be explained by the mesomeric effects depicted in Schemes 1 and 2. In addition, the increased length of the C_4-O_4 double bond may be also explained by a strong intramolecular hydrogen bond between O_4 and O_5H (Table 1). For **FPOMe**, the C_4-O_4 (1.24 Å) and C_2-C_3 (1.34 Å) bond lengths tend toward the expected values for isolated C═O and C═C double bonds, respectively.

Conformational energy investigation of the flavonoid backbone indicated that the lowest potential energy (i.e., that corresponds to a nonplanar conformation) involves a torsion angle $O_1-C_2-C_{1'}-C_{2'}$ of about 22.8°.[15] This torsion angle constitutes a reasonable compromise between attractive (i.e., from a planar structure that provides the framework for an extensive mesomeric effect) and repulsive steric interactions (i.e., that result from the vicinity of the orthohydrogens of the B ring with the C ring). The difference in energy between the lowest energy of the nonplanar conformation versus the planar one is, however, weak (ca. 0.7 kcal mol^{-1}). In the absence of mesomeric driving force, the torsion angle $O_1-C_2-C_{1'}-C_{2'}$ was found to range from 8.52 to 20.01° (e.g., baicalein). The exocyclic oxygen O_4 along with the B-ring substitution pattern are therefore essential to maintain the planarity of the flavone structure. Inducing a partial negative charge on O_4 via hydrogen bonding strengthens the contribution of this mesomeric effect and then contributes to the planarity of the molecule (Scheme 2). On the other hand, baicalein displays a strong hydrogen bond (1.74−1.85 Å for O_5H-O_4) and two weaker hydrogen bonds (2.42−2.54 Å for O_6H-O_5, 2.20−2.23 Å for O_7H-O_6) and adopts an anticlockwise orientation.[16] Salvigenin (1.68 Å for O_5H-O_4) only possesses one strong hydrogen bond. For ladanein, the situation is at odds with a strong hydrogen bond between O_4 and O_5H (1.62−1.71 Å, anticlockwise orientation), whereas O_6H establishes a weaker interaction with O_7CH_3 (2.21−2.33 Å) with a clockwise orientation (see Figure S2).

Acido-Basic Properties. Due to their sparing solubility in water (ca. $10^{-5}-10^{-4}$ M), UV−vis absorption spectrophotometric titrations versus pH of the ladanein analogues were carried out in CH_3OH/H_2O (80/20 w/w). This allowed calculating the protonation constants of the 6-OH unit (Table 2) as well as the electronic spectra of the corresponding protonated species (see Figures S3−S9). The protonation constant of the 5-OH group could not be measured under our experimental conditions. With respect to the 5-OH-flavone (pK_a = 11.44 in dioxane/water 1/1 w/w[17] and pK_a = 11.34 in CH_3OH/water 1/1 w/w[18]), the 5-OH pK_a values were estimated to be >12 due to a strong intramolecular hydrogen bond with the neighboring β-carbonyl group.[19] The acido-basic properties were compared to the rare physicochemical data that are reported for related flavones (scutellarin B = 5,6,4′-trihydroxy-7-*O*-glucuronide-flavone). At first sight, the pK_a values are not markedly influenced by the substituents of the B cycle. For example, **FOMe** displays a slightly more basic 6-OH, which likely originates from the +M directing effect of the 4′-methoxy group (Scheme 1) that affects the 2-phenyl-chromone unit. Similarly, the basicity of the 6-OH function

DOI: 10.1021/acsomega.8b03332
ACS Omega 2019, 4, 4871−4887

Table 1. Solid-State Structural Characteristics[a] of the Flavones Considered in This Work as well as Those Described for Salvigenin and Baicalein

structural parameters	ladanein (natural)	ladanein (synthetic)	final precursor FPOMe	baicalein[7]	salvigenin[8]
$C_2-C_{1'}$ (Å)	1.47	1.46	1.47	1.47/1.47/1.48	1.47
C_2-C_3 (Å)	1.35	1.36	1.34	1.36/1.36/1.35	1.35
C_3-C_4 (Å)	1.44	1.42	1.44	1.43/1.43/1.43	1.43
C_4-O_4 (Å)	1.26	1.26	1.24	1.26/1.26/1.26	1.26
O_5H-O_4 (Å)[b]	1.71	1.62	na	1.81/1.74/1.85	1.68
O_6H-O_5 (Å)[b]				2.43/2.42/2.54	
$O_6H-O_7CH_3$ (Å)[b]	2.21	2.33	2.29	na	
O_7H-O_6 (Å)[b]	na	na	na	2.27/2.20/2.23	
A−C (deg)	1.77	0.27	1.29	0.79/2.46/2.34	0.80
$O_1-C_2-C_{1'}-C_{2'}$ (deg)	2.14	0.93	18.96	20.01/9.13/8.52	4.38

structural parameters	pectolarigenin[9]	cirsimaritin[10]	eupatorin[11]	5,7,3′-trihydroxy-6,4′,5′-trimethoxyflavone[12]	5,6,7,5′-tetramethoxy-3′,4′-methylenedioxy-flavone[13]
$C_2-C_{1'}$ (Å)	1.47	1.47	1.47	1.48	1.47
C_2-C_3 (Å)	1.35	1.35	1.35	1.34	1.35
C_3-C_4 (Å)	1.43	1.43	1.42	1.44	1.44
C_4-O_4 (Å)	1.25	1.26	1.26	1.26	1.24
O_5H-O_4 (Å)[b]	1.85	1.85	1.86	1.85	
O_7H-O_6 (Å)[b]	2.28			2.38	
A−C (deg)	1.51	2.20	2.75	1.37	1.95
$O_1-C_2-C_{1'}-C_{2'}$ (deg)	7.42	22.59	0.04	4.29	0.15

[a]The values have been rounded to two decimal places. [b]The hydrogen positions have been calculated.

DOI: 10.1021/acsomega.8b03332
ACS Omega 2019, 4, 4871−4887

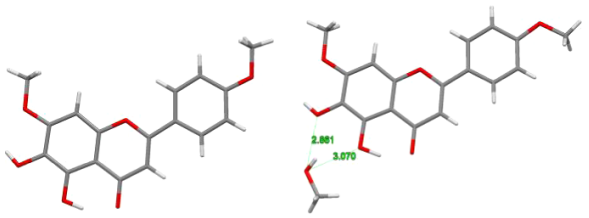

Figure 2. X-ray crystal structures of (A) natural and (B) synthetic ladanein.

Scheme 1. Mesomeric Effects for Ladanein Induced by the 4′-OCH_3

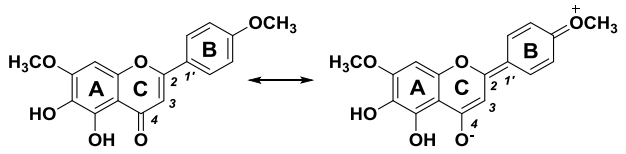

slightly increases in the case of the final precursor **FPOMe** (absence of O_4−HO_5 hydrogen bond) and **FFCF$_3$** (steric interaction). Nevertheless, these differences remain small and under physiological conditions, all flavones display the same neutral state.

Table 3 gathers the absorption spectrophotometric properties of the flavones. For ladanein **FOMe**, we have previously shown that its electronic transitions (highest occupied molecular orbital (HOMO) and lowest unoccupied molecular orbital (LUMO) calculated at the density functional theory (DFT) level, PCM-TD-M06) involved the system as a whole.[5]

The HOMO electronic density is mainly centered on ladanein A ring, whereas that of the LUMO is mostly localized on the B and C rings. The peak at 335 nm measured for ladanein (computed value of 328 nm with a large oscillator strength f = 0.78) was attributed to a HOMO−1−LUMO transition with a small HOMO−LUMO contribution, so that it can be considered as a π−π^* transition with a small charge-transfer (CT) character. In addition, time-dependent DFT experiments predicted a weak HOMO−LUMO transition at 351 nm (f = 0.04) presumably hidden in the foot of the intense band centered at 335 nm.

For **FH**, **FF**, **FCF$_3$**, **FFCF$_3$**, and **FOCF$_3$** that are lacking a (+M) OCH_3 substituent in the B ring (i.e., the B substituents are mainly −I or −M directing groups),[21−23] the pH increase induces weak hypo- or hyperchromic shifts of bands II and I,

Table 2. Protonation Constants (6-OH Group) of the Ladanein Analogues[a]

compounds	log K^h ($\pm\sigma$)
F/flavone	na[b]
FH/negletein	9.75(9)
FOME/ladanein	10.33(5)
salvigenin	nd
POME	10.10(3)
FOCF$_3$	9.47(6)
FF	9.87(5)
FFCF$_3$	10.15(2)
FCF$_3$	10.08(3)
scutellarin B	10.19/7.77[c]

[a]Solvent: CH_3OH/H_2O (80/20 w/w); I = 0.1 M (NEt_4ClO_4); T = 25.0(2) °C. [b]na = not applicable. [c]Phosphate buffers.

respectively (Table 1). Alike **FOMe** and **FPOMe**, an absorption band of significantly lower intensity emerges at ∼450 nm upon deprotonation of the 6-OH unit. This new absorption band is undoubtedly associated to the nature of the B-cycle substituent (λ^{max} = 395 nm for **FPOMe** to 446 nm for **FCF$_3$**) and was attributed (e.g., ladanein[5]) to a HOMO−LUMO transition, the molecular orbital (MO) topology being unaltered for the anionic state with respect to the neutral one, with however a stronger contribution on the deprotonated oxygen in the HOMO. These data are thus in agreement with a resonance effect (Scheme 1) that affects the electronic properties of the molecule (i.e., donor−acceptor system).

Electrochemical Properties. The electrochemical properties of ladanein and its synthetic analogues (Figure 1) were then investigated using cyclic voltammetry (CV). To assess the role of the carbonyl unit of the C ring, 2-phenyl-chromone **F** was used as a model. For the sake of solubility, the electrochemical experiments conducted on **FOMe** and its analogue were carried out in dimethyl sulfoxide (DMSO). First, Figure 3 depicts the CVs of **FOMe** and its analogues that were recorded from −0.8 to 1.2 V. The repetitive scans were found to be reproducible, thus indicating the absence of adsorption processes and degradation products. Regardless of the sweep rate (i.e., 0.05−6 V s^{-1}), **FOMe** is characterized by a chemically irreversible oxidation (wave I) and a broadened irreversible reduction (wave II) in the reverse scan. These features are typical of catechol-based molecules characterized by an ECE-type mechanism (see Figure S10).[24] The comparable CV profiles measured for ladanein and its

Scheme 2. Mesomeric and Prototropic Effects That Can Explain the Structural Features Observed for Ladanein and Its Analogues

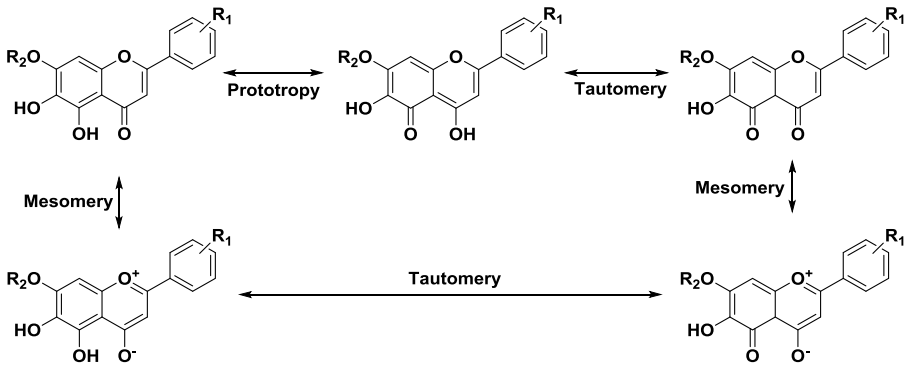

DOI: 10.1021/acsomega.8b03332
ACS Omega 2019, 4, 4871−4887

Table 3. Absorption Characteristics of the Flavones Considered in This Work

	protonated		6-monodeprotonated		
	band I	band II	band I	Band II	additional band
flavone[a]	λ_{max} ($\varepsilon^{\lambda_{max}}$) nm ($10^4$ M^{-1} cm^{-1})				
F/flavone	295 (2.03)	252 (1.68)	na[b]	na	na
FH/negletein	321 (1.57)	277 (2.44)	317 (1.73)	275 (2.05)	423 (0.18)
FOMe/ladanein	335 (3.19)	286 (2.65)	322 (2.98)	303 (2.94)	424 (0.26)
salvigenin	332 (3.35)	276 (2.45)	na	na	na
FPOMe	325 (3.02)	277 (2.01)	301 (3.04)		395 (0.61)
FOCF$_3$	321 (1.04)	277 (1.71)	314 (1.16)	278 (1.35)	424 (0.11)
FF	321 (1.29)	278 (2.00)	315 (1.40)	280 (1.70)	405 (0.15)
FFCF$_3$	320 (1.17)	273 (2.01)	326 (1.33)	262 (2.13)	450 (0.19)
FCF$_3$	322 (1.52)	277 (2.74)	326 (1.73)	272 (2.40)	446 (0.22)
apigenin[c]	338 (2.11)	268 (1.85)	na	na	na

[a]Solvent: CH_3OH/H_2O (80/20 w/w); I = 0.1 M NEt_4ClO_4; T = 25(2) °C. The errors on the λ and ε are estimated to be ±1 nm and 10%, respectively. [b]na = not applicable. [c]Solvent: CH_3OH/H_2O (80/20 w/w); I = 0.1 M $NaClO_4$ (see ref 20).

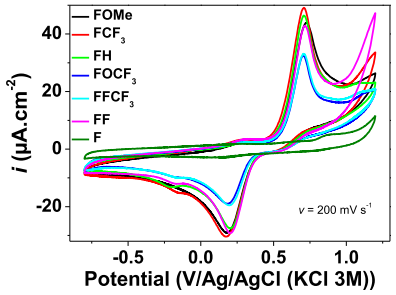

Figure 3. CV of **FOMe** compared to that of its synthetic analogues. Cyclic voltammograms measured for ∼2−2.5 mM flavone in DMSO at a sweep rate of 200 mV s^{-1}. Solvent: DMSO; I = 0.1 M n-Bu_4NPF_6; T = 25 °C; reference electrode = KCl(3 M)/Ag/AgCl; working electrode = glassy carbon (GC) disk of 0.07 cm^2 area; counter-electrode = Pt wire.

analogues (Figure 3) suggest that a common electrochemical behavior is shared and dominates whatever the substitution on the B ring (vide supra, acido-basic properties). The comparison with 2-phenyl-chromone **F** further established that the redox processes are related to the A ring containing the catechol-type moiety.

The linear dependencies of $\log(i_p)$ versus $\log(v)$ indicated that the redox processes are diffusion-controlled in DMSO (i.e., the slope value of the linear $\log(i_p) = f(\log(v))$ variation ranges from 0.48 to 0.63; see Table S1 and Figures S11−S17). A slope value of ∼0.5 reflects diffusion-controlled electrode processes, whereas a slope value close to 1.0 indicates adsorption-controlled processes.[25] For most of the flavones, the variation of E_{pa} (or E_{pc}) as a function of $\log(v)$ (see Table S1 and Figures S18−S24) suggested a mixed kinetic control by both an electron transfer and a chemical reaction. Kinetic control by slow electron transfer (i.e., overpotential process induced by limited reaction kinetics) is evidenced at higher sweep rates.[26]

For instance, this process was already reported for catechol, caffeic acid,[27] dihydrocaffeic acid, and caffeic acid phenethyl ester in DMSO[24] and is not influenced by the structural differences among these four compounds. It results from the competition between deprotonation and radical cation delocalization, with the first process being the most favored one. We then examined the dependence of the current function ($i_p/v^{1/2}$) on v, which is another diagnostic criterion to the mechanism of electron transfer.[28] For simple reversible or irreversible reactions, horizontal variations are expected, whereas increase (or decrease) of ($i_p/v^{1/2}$) with v is related to charge transfers coupled with chemical reactions.[28] Regardless of the flavone, the variation of ($i_p/v^{1/2}$) as a function of v (see Figures S25−S30) clearly supported coupled charge transfers related with chemical reactions. The ($i_p/v^{1/2}$) ratios vary for v < ∼1 V s^{-1} (i.e., coupled chemical reaction following an electron transfer), whereas a mechanism transition was observed with no marked variation for v > 1 V (i.e., deprotonation that alters the electron transfer kinetics; reaction overpotential).

To better address this rate-determining step, a Tafel parameter (noted b) was next evaluated for ladanein **FOMe** (see Figure S31) using the following equation[29] valid for an irreversible diffusion-controlled process.

$$E_p = \frac{b}{2} \times \log(v) + \text{constant with } b = \frac{2.303RT}{\beta n_\beta F} \quad (1)$$

with βn_β (i.e., charge-transfer coefficient with β = symmetry factor and n_β = total number of electrons transferred in this charge-transfer step). The rate constant of the chemical reaction (i.e., deprotonation) following the electron transfer can be thus evaluated ($k_H = 0.1(Fv_i/RT)$) where v_i is the scan rate at the intercept of the two straight lines. For **FOMe**, the rates of the chemical reaction (i.e., deprotonation of phenols) were estimated to be ∼2.8 and 3.0 s^{-1} for the anodic and cathodic processes, respectively.

For an irreversible process, it is expected (eq 1) that the cathodic (or anodic) shift in peak potential (or half-peak potential) is ∼30 mV/βn_β. Assuming only the sweep rates ranging from 0.050 to 1 V s^{-1}, the βn_β values for the cathodic signals were found to be close to the theoretical value (i.e., βn_β = 0.5 for an elementary $1e^-$ transfer with n_β = 1 and β = 0.5).[28] For the anodic signals, the βn_β values are close to a theoretical value of βn_β = 0.25. This approach is valid only if the electrode process consists of a single elementary step that involves the simultaneous release of electrons from the electrode to the reactant. In most cases, an electrode process consists of a sequence of consecutive (or parallel) elementary electron transfers and chemical reactions. In this context, the above approach is formally correct only if the first step of the sequence imposes the rate of the whole process and involves the simultaneous release of n electrons from the electrode.[30]

DOI: 10.1021/acsomega.8b03332
ACS Omega 2019, 4, 4871−4887

To diagnose the irreversibility of our systems and evaluate the charge-transfer coefficients, the following equation[31] was then used[28]

$$E_p - \frac{E_p}{2} = 1.857\frac{RT}{\beta n_\beta} \quad (2)$$

with $E_p = E_{pa}$ (or E_{pc}), $E_{p/2}$ = the potential determined at $i_{p/2}$, and βn_β, the charge-transfer coefficient (see Figures S32−S38). In a multistep electrode process characterized by a sequence of consecutive elementary steps, the electrode kinetics is affected only by the rate-determining step and by the steps that precede it. The electrode kinetics is not controlled by the following steps that may involve further electron transfers (i.e., not the case herein). For ladanein (see Table S1 for the other flavones), the charge-transfer coefficients βn_β were calculated to be 0.44 and 0.40 for the anodic and cathodic signals, respectively. Assuming a $1e^-$ transfer in the limiting charge-transfer process, the factor coefficient was estimated to be close to 0.5 for both the cathodic and anodic processes, in agreement with the measured data above.

Figure 4 now depicts the variation of i_{pa} and i_{pc} for ladanein as a function of $v^{0.5}$.

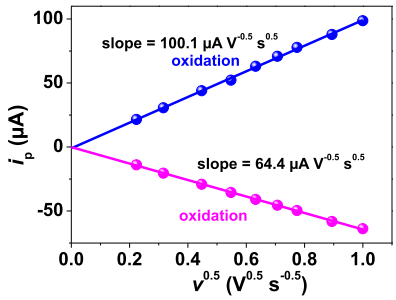

Figure 4. Variation of i_{pa} and i_{pc} as a function of the square root of v (v = sweep rate in mV s^{-1}) for ladanein (2.32 mM). Solvent: DMSO; I = 0.1 M n-Bu_4NPF_6; T = 25 °C; reference electrode = KCl(3 M)/Ag/AgCl; working electrode = GC disk of 0.07 cm^2 area; counterelectrode = Pt wire.

No adsorption processes are expected since i_{pa} and i_{pc} follow a linear dependence with the ordinate at the origin being equal to 0, thus confirming diffusion-controlled reactions. The current intensity i_p for an irreversible system can be expressed as follows

$$i_p = 2.99 \times 10^5 n(\beta n_\beta)^{0.5} A C_0 D^{0.5} v^{0.5} \quad (3)$$

where A is the area of the working electrode (0.07 cm^2), n is the total number of electrons exchanged, βn_β is the charge-transfer coefficient, D_0 is the diffusion coefficient (cm^2 s^{-1}), C_0 is the concentration of the electroactive species (mol cm^{-3}), and v is the sweep rate (V s^{-1}).

Using βn_β values for the anodic and the cathodic processes (see Table S1) and using the D_0 value (i.e., from diffusion-ordered spectroscopy NMR, 2.34×10^{-6} cm^2 s^{-1} for ladanein, Figure S39), the total number of electrons involved in the anodic and cathodic process was estimated to be close to 2 (see Table S2). The differences observed can be explained by the inaccurate estimates of the $n(\beta n_\beta)$ and D_0 values rather than a different electrochemical behavior. These electrochemical data are therefore in agreement with a $2e^-$ oxidation/deprotonation ECE of the A-catechol, with the first electron transfer being the rate-limiting step (Scheme 3). The electrochemical response of **FOMe** and its analogues in DMSO is similar to that measured for closely related compounds (vide supra).

Scheme 3. Suggested Electrochemical Behavior of Ladanein and Its Analogues within the Potential Range Considered (from −1.2 to 0.8 V) in DMSO

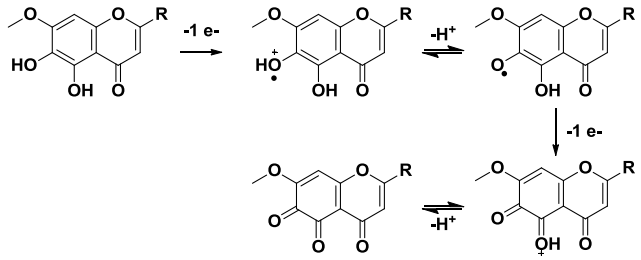

From −2.35 to −1 V, an additional quasireversible electrochemical signal was observed (Figure 5) and was

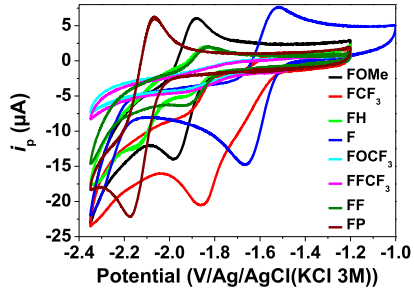

Figure 5. CVs of the flavones that demonstrate the effect of the substitution of the B ring on the quasireversible signal arising from the carbonyl unit. Solvent: DMSO; I = 0.1 M n-Bu_4NPF_6; T = 25°C; v = 200 mV s^{-1}; reference electrode = KCl(3 M)/Ag/AgCl; working electrode = GC disk of 0.07 cm^2 area; counterelectrode = Pt wire.

attributed to the C-ring enone moiety in agreement with 2-phenyl-chromone (see Figures S40−S41). The anodic (E_{pa})-to-cathodic (E_{pc}) peak separations (ΔE_p) were found to be higher than expected for reversible one-electron transfer, thus substantiating quasireversibility of the corresponding redox process (see Table S3 and Figures S42−S48). In most cases, the i_{pa}-to-i_{pc} ratios were found to be lower than 1, also in agreement with a quasireversible process (see Table S3). This likely originates from disproportionation or side reactions (e.g., dimerization, vide infra). Regardless of the flavone considered, the intensities of the cathodic (i_{pc}) and anodic (i_{pa}) signals vary linearly with $v^{0.5}$ in agreement with a (quasi)reversible behavior. These redox reactions are diffusion-controlled and suggest the absence of adsorption processes (see Figures S49−S55). With the exception of the final precursor (**FPOMe**), the $E_{1/2}$ sequence (see Table S3) fairly follows the λ_{max} sequence of either band I or band II (vide supra), confirming the key role of the carbonyl group in each of these processes.

Literature data indicated that the 2-phenyl-chromone is characterized by a one-electron reversible wave ($E_{1/2}$ at −2.28 V) and a two-electron wave ($E_{1/2}$ at −2.85 V vs Ag/Ag^+ in dimethylformamide (DMF) at 298 K).[32] On the other hand, electrochemical measurements on 7-acetoxyflavone and 7-hydroxyfavone showed a two-electron irreversible reduction at E_{pc} = −1.77 and −1.44 V/CSE, respectively (i.e., DMF at v =

DOI: 10.1021/acsomega.8b03332
ACS Omega 2019, 4, 4871−4887

200 mV s^{-1}).[33] These diffusion-controlled electrode processes were found to be influenced by the substituents due to extended conjugation, as observed for our ladanein analogues. Under our experimental conditions, a single quasireversible signal ($E_{1/2}$ = −1.59 V/KCl(3 M)/Ag/AgCl) was evidenced for **F**. This apparent one-electron process is proposed to lead to a monoradical species, which was confirmed in previous studies by electron paramagnetic resonance spectroscopy. No additional redox signal was evidenced when the potential range was expanded to values that are more negative. The reversible redox wave observed for **FOMe** (i.e., $E_{1/2}$ = −1.93 V/KCl(3 M)/Ag/AgCl measured at 200 mV) was therefore proposed to be associated with the reduction of the flavone carbonyl (Scheme 4). A cathodic shift of ∼340 mV is indeed observed

Scheme 4. Suggested Side Reactions upon One-Electron Reduction of the Enone Unit[a]

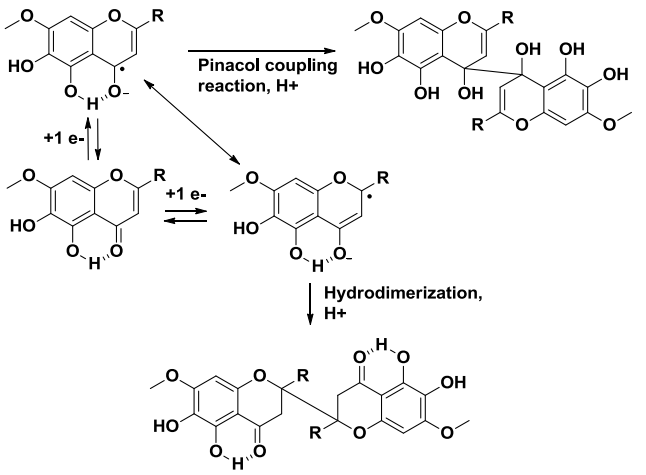

[a]The reduction of the carbonyl unit is likely the plausible redox pathway.

between **FOMe** and **F**. This property is mainly due to the electronic effects of the substituents on the A and B rings as well as the hydrogen bond between the carbonyl and 5-OH groups. The comparison of **FH** to **F** also shows a cathodic shift of 280 mV, thus demonstrating that the substitution pattern of A ring induces the largest shift, whereas the methoxylation of the B ring only shifts the $E_{1/2}$ value of about 60 mV with respect to **FH**. Withdrawing of the hydrogen bond with the β-carbonyl by methylation of the 5-OH (**FPOMe**) induces an extra cathodic shift of 190 mV with respect to ladanein **FOMe**. This suggests that **FPOMe** is electrochemically more inert with respect to carbonyl reduction and highlights the key role of this hydrogen bond in the electrochemical activation/behavior of the flavone.

In contrast to the above experiments, scanning the potential from −2.35 to 1.2 V alters the CV behavior of ladanein **FOMe** and its analogues with the presence of additional reduction and oxidation signals (Figure 6).

A new anodic peak markedly appears at −0.11 V, whereas the catechol-centered anodic peak is shifted from 0.72 to 0.64 V. In addition, three new cathodic peaks appear at −0.30, −1.07, and −1.62 V. Last, the reduction peak (i.e., centered on A ring) is also shifted from 0.18 to 0.23 V. This peculiar electrochemical behavior can be related to the formation of degradation products (e.g., resulting from pinacol coupling

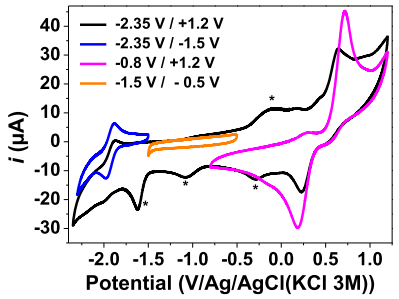

Figure 6. CV of **FOMe** (2.32 mM) showing the formation of additional electrochemical signals when scanning the potential from −2.35 to 1.2 V. Solvent: DMSO; I = 0.1 M n-Bu_4NPF_6; T = 25°C; v = 200 mV s^{-1}; reference electrode = KCl(3 M)/Ag/AgCl; working electrode = GC disk of 0.07 cm^2 area; counterelectrode = Pt wire.

reaction[34] or hydrodimerization[35]) of two radicals formed upon reduction of the enone unit, as shown in Scheme 4.

Iron Coordination Properties. Previously,[5] we have shown that ladanein affords monoferric monochelates under acidic conditions (i.e., employed to prevent the formation of insoluble (hydr)oxo Fe(III) species). Of the two bidentate binding sites, the β-hydroxy-ketone group of ladanein was shown to be the most effective one. Monoferric monochelates under protonated and hydroxylated states were also evidenced and quantified. The pFe value calculated for **FOMe** was compared to that of relevant natural chelators (e.g., polyphenols, siderophores, etc.) and emphasized that the moderate Fe(III) binding capability of ladanein is in excellent agreement with the ability of ferrioxamine B (DFO) to inhibit its antiviral activity.[5] To go a step further, we provide in Table 4 spectroscopic properties as well as conditional stability

Table 4. Conditional Stability Constants of the Ferric Complexes with Ladanein and Its Analogues[a]

complex	log K^*_{FFe}	λ_{max} LMCT (nm) $\varepsilon^{\lambda_{max}}$ (M^{-1} cm^{-1})
FOMe·Fe[5]	6.0(3)	633(1560)
FH·Fe	5.4(6)	635(1200)
$FFCF_3$·Fe	5.8(4)	651(1050)
FCF_3·Fe	5.3(6)	650(1230)
FF·Fe	4.7(3)	655(910)
$FOCF_3$·Fe	5.8(3)	649(1040)
salvigenin[5]	5.8(2)	600(2100)
apigenin[5]	5.5(1)	520(2080)

[a]Solvent: CH_3OH/H_2O (80/20 w/w); I = 0.1 M (NEt_4ClO_4); T = 25.0(2) °C; $[H^+] = 10^{-2}$ M. Error = 3σ with σ = standard deviation (SD).

constants of the metal complexes with the ladanein analogues that were measured at pH 2.0. With the exception of **FF**, the analogues are characterized by binding affinities for Fe(III) similar to **FOMe**. For analogues displaying an electron-withdrawing substituent on the B ring (**$FFCF_3$**, **FCF_3**, **FF**, and **$FOCF_3$**), the ligand-to-metal charge transfer (LMCT) is bathochromically shifted by ∼20 nm in regard to **FOMe** or **FH**. This can be ascribed to the electronic impacts induced by these substituents on the carbonyl unit. These observations substantiate the key role of the carbonyl group in Fe(III) complexation and confirm the role of the β-hydroxy-carbonyl unit as the relevant bidentate binding site.

To mimic the physiological conditions, the Fe(III) binding abilities of ladanein and its analogues were next examined at

DOI: 10.1021/acsomega.8b03332
ACS Omega 2019, 4, 4871−4887

pH 7.4 in a CH_3OH/H_2O solvent (80/20 w/w). Nitrilotriacetic acid **NTA** was employed as a supporting ligand to prevent Fe(III) hydrolysis into insoluble species (at pH 7.4, $\log K^*_{FeNTA} = 6.0(3)$; see Figure S56).[5] For instance, Figure 7

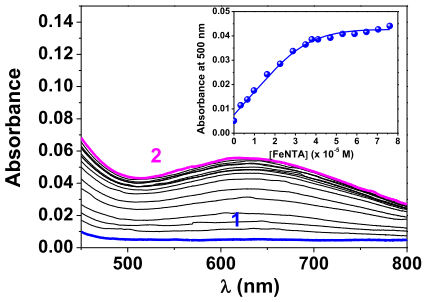

Figure 7. Absorption spectrophotometric titration of the ladanein analogue **FFCF$_3$**. The inset shows the variation of the absorbance at 500 nm vs [Fe**NTA**]. Solvent: CH_3OH/H_2O (80/20 w/w); pH = 7.4 [*N*-(2-hydroxyethyl)piperazine-*N*′-ethanesulfonic acid (HEPES)]; I = 0.1 M (HEPES); T = 25.0(2) °C; l = 1 cm. $[\mathbf{FFCF_3}]_0 = 3.80 \times 10^{-5}$ M.

depicts the UV−vis absorption titration of **FFCF$_3$** as a function of $[\mathbf{FeNTA}]_0$ (see Figures S57−S62). Regardless of the flavone employed, ternary flavone·Fe**NTA** complexes were systematically characterized and quantified.

To go further and confirm the formation of the ternary ferric complexes, electrospray mass spectra were recorded (negative mode). Regardless of the flavone, ternary Fe(III) complexes were characterized (Table 5 and see Figure S63 for **FOMe**) in

Table 5. ESI-MS Monoisotopic Ions (Intensity Maxima) of the Ferric Ternary Complexes with Ladanein FOMe and Its Analogues

species	m/z experimental value	m/z theoretical
[Fe**NTA**−H]$^-$	not measured	240.95
[**FOMe**−H + Fe**NTA**]$^-$	554.80	555.03
[**FH**−H + Fe**NTA**]$^-$	524.75	525.02
[**FH**−H + 2Fe**NTA**]$^-$	768.6	768.97
[**FOCF$_3$**−H + Fe**NTA**]$^-$	608.75	609.00
[**FOCF$_3$**−H + 2Fe**NTA**]$^-$	852.50	852.95
[**FFCF$_3$**−H + Fe**NTA**]$^-$	610.75	611.00
[**FCF$_3$**−H + Fe**NTA**]$^-$	592.80	593.00
[**FF**−H + Fe**NTA**]$^-$	542.75	543.01
[**FF**−H + 2Fe**NTA**]$^-$	786.60	786.96

agreement with the absorption spectrophotometric study. For **FH**, **FOCF$_3$**, and **FF**, other ferric species involving additional Fe**NTA** units were also characterized and likely originate from adducts induced by the electrospray ionization mass spectrometry (ESI-MS) conditions.

The binding constants and absorption spectroscopic parameters have been gathered in Table 6. Similar to catecholate-based ligands,[36] the LMCT absorptions of the ternary complexes lie at much higher energies. The presence of **NTA** induces a hypsochromic shift of the LMCT absorptions that ranges from 31 nm (**FFCF$_3$**) to 62 nm (**FOMe**). With the trianionic **NTA**, the Lewis acidity of the metallic center significantly decreased and its *d* orbitals are therefore destabilized. This effect is significant for flavones displaying electron-donating groups (**FOMe**), whereas it remains limited for flavones with electron-withdrawing substitution (**FFCF$_3$** and **FCF$_3$**).

Even though the stability constants related to Fe**NTA** binding are close within the given experimental errors, ladanein **FOMe** seems to be among the less active binders as its constant was found to be the lowest one with respect to that of its synthetic analogues. Electron-withdrawing substitutions in the B ring seemingly strengthen Fe**NTA** binding, the more efficient binder from the ladanein analogue series being the **FFCF$_3$** system (Table 6 and Figure 7).

Uptake of Fe(III) by Ladanein under Acidic Conditions. Using stopped-flow spectrophotometry, kinetic studies were first performed under acidic conditions. Under these experimental conditions, the $\mathbf{LHFe}^{2+}$ complex (i.e., **L** = fully deprotonated state of ladanein **FOMe**) corresponds to the predominant ferric complex, whereas Fe^{3+} and $Fe(OH)^{2+}$ are the major free iron(III) species (see Figure S64, $K_{Fe(OH)^{2+}} = 10^{-1.39}$).[37] The formation kinetics was monitored under pseudo-first-order conditions ($[Fe^{3+}]_0 > 10 \times [\mathbf{FOMe}]_0$) at λ = 650 nm, which corresponds to the largest absorption spectrophotometric difference between the reactants (Fe^{3+} + LH_2) and the product $\mathbf{LHFe}^{2+}$. A single rate-limiting step was evidenced in the second time span, and no signal loss was observed during the dead time (∼3 ms) of the kinetic device (Figure 8). The absorbances at the end of the rate-limiting step satisfactorily correspond to the calculated values for the $\mathbf{LHFe}^{2+}$ complex. In all cases, the absorbance followed an exponential growth versus time, indicating first-order kinetics ($v = -d[\mathbf{L}]/dt = k_{obs}[\mathbf{L}]$) with respect to the ligand. A slower biphasic kinetic process (i.e., minute time span) likely related to the iron(III)-mediated oxidation of ladanein was also observed (Figure 8). This suggests that Fe(III) complexation leads to flavone oxidation even under acidic conditions, whereas the free ligand remained unaltered over a long period in the absence of Fe(III) under these experimental conditions. This substantiates that Fe(III) chelation might favor specific

Table 6. Successive Stability Constants of the Ferric NTA Complexes with Ladanein and Its Analogues[a]

flavone	$\log K^*_{L\text{·}FeNTA}$ (3σ)	λ_{max} LMCT (nm) $\varepsilon^{\lambda_{max}}$ (M^{-1} cm^{-1})
FPOMe/final precursor	nc	na
F/flavone	nc	na
FOMe/ladanein	4.7(4)/4.9(6)	571(2170)
FFCF$_3$	5.7(1)	620(1300)
FCF$_3$	4.4(1)	615(2300)
FF	5.0(1)	600(900)
salvigenin	5.8(7)	∼510[b]

[a]Solvent: CH_3OH/H_2O (80/20 w/w); pH = 7.4 (HEPES); I = 0.1 M (HEPES); T = 25.0(2) °C. nc = no complexation. Error = 3σ with σ = standard deviation. [b]Partially masked by the flavone transitions.

DOI: 10.1021/acsomega.8b03332
ACS Omega 2019, 4, 4871−4887

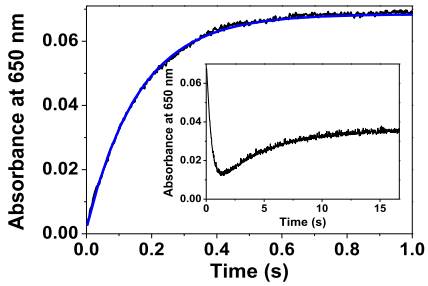

Figure 8. Variation of the absorbance (LMCT at 650 nm) as a function of time for the formation of ladanein ferric complexes. The inset shows the variation of the absorbance at 650 nm that likely corresponds to the slower oxidation of ladanein mediated by iron(III) complexation. Solvent: CH_3OH/H_2O (80/20 w/w); I = 0.1 M (NEt_4ClO_4); T = 25.0 ± 2 °C; $[H^+]_0$ = 0.032 M; $[\mathbf{FOMe}]_0 = 3.83 \times 10^{-5}$ M; $[Fe]_0 = 3.09 \times 10^{-4}$ M.

C,C- (or C,O) oxidative coupling reactions or auto-oxidation processes.[38]

For $[H^+]_0$ ranging from 9.4×10^{-3} to 3.2×10^{-2} M, $[Fe(III)]_0$ (i.e., in excess) was varied and the pseudo-first-order rate constants (k_{obs}) were calculated (see Figure S65). Under these experimental conditions, Fe^{3+} and $Fe(OH)^{2+}$ predominate in solution and ladanein is fully protonated (LH_2). The following mechanism can therefore be suggested

$$Fe(H_2O)_6^{3+} \overset{K_H fast}{\rightleftharpoons} Fe(H_2O)_5(OH)^{2+} + H^+ \quad (4)$$

$$Fe^{3+} + \mathbf{L}H_2 \xrightarrow{k_{Fe^{3+}}} \mathbf{L}HFe^+ + H^+ \quad (5)$$

$$Fe(OH)^{2+} + LH_2 \xrightarrow{k_{Fe(OH)^{2+}}} \mathbf{L}HFe^+ + H_2O \quad (6)$$

The rate law relative to LH_2 is hence

$$v = -\frac{d[\mathbf{L}H_2]}{dt} = k_{Fe^{3+}}[Fe^{3+}][\mathbf{L}H_2] + k_{Fe(OH)^{2+}}[Fe(OH)^{2+}][\mathbf{L}H_2]$$

$$v = -\frac{d[\mathbf{L}H_2]}{dt} = k_{obs}[\mathbf{L}H_2] \quad (7)$$

which becomes eq 5 if $[Fe^{3+}]$ and $[Fe(OH)^{2+}]$ are expressed as a function of K_H and $[Fe(III)]_0$.

$$v = \left(\frac{k_{Fe^{3+}}[H^+] + k_{Fe(OH)^{2+}}K_H}{[H^+] + K_H}\right)[Fe(III)]_0[\mathbf{L}H_2]$$

$$v = k_a[Fe(III)]_0 \times [\mathbf{L}H_2] \quad (8)$$

Figure 9 presents the variation of k_a versus $[H^+]_0$ according to eq 5. $\mathbf{L}HFe^+$ is formed through two pathways involving either Fe^{3+} ($k_{Fe^{3+}} = 4.3(1.6) \times 10^2$ M^{-1} s^{-1}) or $Fe(OH)^{2+}$ ($k_{Fe(OH)^{2+}} = 2.7(2) \times 10^3$ M^{-1} s^{-1}). The $k_{Fe^{3+}}$ value reflects an associative ligand interchange mechanism (I_a) and is dependent on the nature of the incoming ligand that substitutes the first water molecule (Table 7).[39,40] By contrast, $Fe(OH)^{2+}$ undergoes a dissociative ligand interchange mechanism (I_d) (Eigen–Wilkins) and its rate-limiting step corresponds to the loss of the first water molecule (i.e., not dependent on the nature of the entering ligand).[41,42] The $k_{Fe(OH)^{2+}}$ rate constant measured for the ladanein ferric complex compares well with those

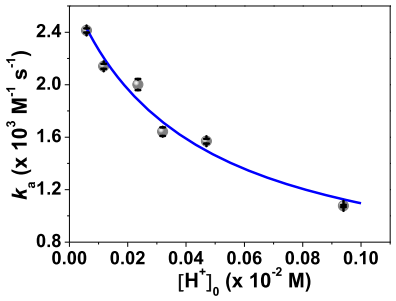

Figure 9. Formation kinetics of the ladanein ferric complex: variation of k_a (see eq 8) vs $[H^+]_0$. Solvent: CH_3OH/H_2O (80/20 w/w); I = 0.1 M; T = 25.0(2) °C. Uncertainties are given as 3σ.

Table 7. Reactivity of Various Ferric Species with Catecholate, Hydroxamate, Hydroxycarboxylate, and Phosphate-Based Chelators

ligands	$k_{Fe^{3+}}$ (M^{-1} s^{-1})	$k_{Fe(OH)^{2+}}$ (10^3 M^{-1} s^{-1})	$k_{FeNTA(OH)}$ (10^4 M^{-1} s^{-1})
ferrioxamine B[43,44]		3.6	
pyoverdine PaA[45]	<80	7.7(4)	6.2(3)[a]
FOMe/ladanein[a]	430(160)	2.72(2)	0.84(3)
$\mathbf{FCF_3}$[a]			1.9(2)
$\mathbf{FFCF_3}$[a]			2.9(4)
apigenin[a]	800(200)	2.0(3)	
catechin[20,46]	90(4)	3.1(2)	2.05(5)
		3.3(2)	
catechol[47]		3.1(2)	
phenol[48]		1.5	
tiron[49,50]		3.08(0.48)	2.7(2)[a]
salicylic acid[50]		3.5	
2,3-dihydroxybenzoic acid		4.8	
phosphate[51]			2.4(4)
tartaric acid		5.1	
citric acid		3.1	
acetohydroxamic acid[51,52]		5.65(0.864)	3.8(3)

[a]This work.

reported for siderophores, polyphenols, or hydroxycarboxylate chelators (Table 7).[39]

Formation Kinetics of the Flavone·FeNTA Complexes. The Fe(III) binding kinetics by natural chelators (e.g., polyphenols, siderophores) or analogues have been extensively investigated under acidic conditions.[41,42] Such conditions are convenient but far from being relevant to account for physiological conditions. In the human body, Fe(III) is usually exposed to pH 7.4 and always bound to proteins (e.g., hemoglobin, transferrin) or low-molecular-weight moderate chelators (e.g., citrate) to maintain its solubility. In model systems, polyamino-carboxylate-based chelators, such as citrate and **NTA**, are therefore used to ensure iron solubility.[51,53−57] **NTA** is a relevant citrate model and belongs to the most studied organic chelators.[58,59] The Fe(III) uptake kinetics by ladanein, two of its analogues (i.e., $\mathbf{FCF_3}$, $\mathbf{FFCF_3}$), and apigenin were then investigated at pH 7.4 (physiological conditions) in the presence of **NTA**. The kinetic study was carried out in excess flavone (i.e., pseudo-first-order conditions) with 1 equiv of **NTA** with respect to the ferric cation. A single exponential signal was observed for **FOMe**, apigenin, and $\mathbf{FCF_3}$, whereas a two rate-limiting step sequence was evidenced for $\mathbf{FFCF_3}$ (Figures 10 and S66−S68). The extrapolated initial absorbances match very well with the

DOI: 10.1021/acsomega.8b03332
ACS Omega 2019, 4, 4871−4887

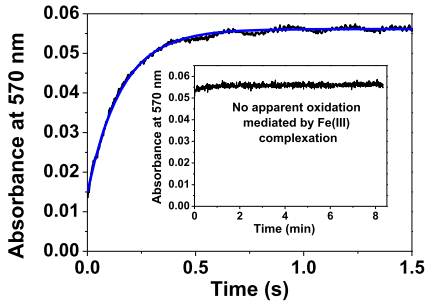

Figure 10. Variation of the absorbance (LMCT at 570 nm) as a function of time for the formation of the ternary ferric complex with ladanein and **NTA**. Inset shows the absorbance variation over a much longer time, demonstrating the absence of oxidation of ladanein triggered by Fe(III) complexation. Solvent: CH_3OH/H_2O (80/20 w/w); I = 0.1 M (NEt_4ClO_4); T = 25.0 ± 2 °C; pH = 7.4 (0.1 M HEPES); $[FeNTA]_0 = 2.30 \times 10^{-5}$ M; $[FOMe]_0 = 5.82 \times 10^{-4}$ M.

absorbances of the reagents (flavone + Fe**NTA**), thus demonstrating that no fast step was lost during the mixing of the reagents (~3 ms). The final absorbance values agreed very well with the values calculated for these ternary complexes flavone·Fe**NTA**. Interestingly, no oxidation of the flavones (Figure 10) was observed. This is in contrast to the observations made for **FOMe** with Fe(III) under acidic conditions (vide supra). This indicates that **NTA** binding likely alters the redox properties of the metal complexes, as suggested by the hypsochromic shift of the LMCT band (Table 6). Auxiliary ligands seemingly shield ladanein from spontaneous Fe-promoted oxidation and can thus constitute a simple and useful method to improve its bioavailability and activity in vivo.

For the investigated flavones, the rate-limiting step (in the second range) likely leads to the formation of a kinetic intermediate flavone·Fe**NTA*** that rapidly rearranges in a subsequent step to the final thermodynamic ternary complex flavone·Fe**NTA**.

$$\text{Fe}\mathbf{NTA} + \mathbf{L} \underset{k_{-1}}{\overset{k_1}{\rightleftarrows}} \mathbf{L}\cdot\text{Fe}\mathbf{NTA}^* \text{ and } \mathbf{L}\cdot\text{Fe}\mathbf{NTA}^* \xrightarrow{k_2} \mathbf{L}\cdot\text{Fe}\mathbf{NTA} \quad (9)$$

For **FFCF$_3$**, the rearrangement step was found to be much slower and resulted in a second first-order step that can be monitored. In that latter case, 2′-fluorine substitution likely induces steric interactions and subsequently large dihedral angle deformation between the B and C rings. The pseudo-first-order rate constants k_{obs1} of the first step vary linearly with $[flavone]_0$ with a significant ordinate at the origin (k_{-1}, monomolecular dissociation rate constant, Table 8, Figures 11 and S69–S71).

The linear least-square fits of k_{obs} versus $[flavone]_0$ led also to the determination of the bimolecular formation rate constant k_1 related to the formation of the ternary intermediate complexes (Table 8).

The k_1/k_{-1} ratio (Table 6) accounts for the stability of the intermediate ferric complexes. For ladanein **FOMe**, the $\log(k_1/k_{-1})$ = 4.0 was found to be close to the conditional stability constant measured at pH 7.4 by UV–vis absorption spectrophotometry ($\log K^*_{\text{FOMe·FeNTA}}$ = 4.7(4)), thus suggesting that the intermediate complex closely resembles the thermodynamic one. For apigenin and **FCF$_3$**, the ratio k_1/k_{-1} is 1–2 orders of magnitude lower than the stability constants measured at pH 7.4 (Table 6), suggesting that the observed

Table 8. Kinetic Parameters[a] Related to the Formation of the FeNTA Complexes with Ladanein and Its Analogues[b]

	first step		second step		
flavone **F**	k_1 ($\times 10^3$ m^{-1} s^{-1})	k_{-1} (s^{-1})	k_2 (s^{-1})	$\log(k_1/k_{-1})$	$k^*_{\text{1-FeNTA}}$
apigenin	4.5(5)	1.3(4)	nd	3.5	5.8(7)
FCF$_3$	1.9(2)	0.6(2)	nd	3.5	4.4(1)
FFCF$_3$	2.9(4)	1.8(3)	0.15(3)	3.2	5.7(1)
FOME	8.4(4)	0.9(3)	nd	4.0	4.7(4)

[a] k_1 and k_{-1} forward and backward rate constants of the formation step; k_2: forward rate constant of the rearrangement step. [b] Solvent: CH_3OH/H_2O (80/20 w/w); pH = 7.4 (HEPES buffer); I = 0.1 M (HEPES); T = 25.0(2) °C. na = not applicable.

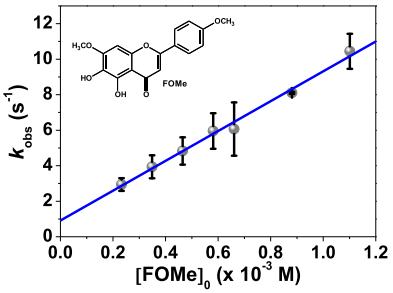

Figure 11. Formation kinetics of **FOMe** ferric complex with Fe**NTA**: variation of the pseudo-first-order rate constant vs $[\mathbf{FOMe}]_0$. $[FeNTA]_0 = 2.30 \times 10^{-5}$ M; solvent: CH_3OH/H_2O (80/20 w/w); I = 0.1 M (NEt_4ClO_4); T = 25.0(2) °C; pH = 7.4 (0.1 M HEPES). Uncertainties are given as 3σ.

rate-limiting step likely leads to a kinetic intermediate that rearranges rapidly to the thermodynamic complex. Evidence of this mechanism came with **FFCF$_3$** for which two rate-limiting steps were observed. If the first rate-limiting step is not significantly dependent on the nature of the flavone, A or B substitution can markedly influence the rearrangement step. Throughout this study, we have assumed a single Fe(III) **NTA** species that, in fact, corresponds to a mixture of two predominant hydroxylated species, namely, the mono-hydroxo $[\text{Fe}\mathbf{NTA}(OH)]^-$ and bis-hydroxo $[\text{Fe}\mathbf{NTA}(OH)_2]^{2-}$ species. Only the $[\text{Fe}\mathbf{NTA}(OH)]^-$ species has been shown to be reactive.[51] Therefore, the k_1 value reflects the reactivity of the flavones with $[\text{Fe}\mathbf{NTA}(OH)]^-$. Table 7 shows the main results obtained for our flavones together with literature data that allowed us to draw important conclusions. The difference observed for **FOMe** and its fluorinated analogues can be explained by the different experimental conditions (CH_3OH/H_2O vs H_2O). The reactivity of $[\text{Fe}\mathbf{NTA}(OH)]^-$ is seemingly independent of the nature of the binding ligand. This suggests that $[\text{Fe}\mathbf{NTA}(OH)]^-$ is associated to a dissociative interchange mechanism of the Eigen–Wilkins type in the same way as $Fe(OH)^{2+}$. $[\text{Fe}\mathbf{NTA}(OH)]^-$ was found to be 4–10 times more reactive than $Fe(OH)^{2+}$, thus accounting for a strong labilizing effect of the water molecules by the trianionic tetradentate **NTA** in the first coordination shell of Fe(III). An increased number of negative charges around the ferric center will indeed strongly destabilize the remaining bound water molecules.

Fe(III) Coordination and pH Dependency as Key Parameters for Ladanein Bioactivation and Inhibition of HCV Entry. From the acido-basic properties, we have seen that, regardless of the flavone considered, the neutral species

DOI: 10.1021/acsomega.8b03332
ACS Omega 2019, 4, 4871–4887

predominates over a broad pH range from 5 to 7.4, which is a relevant condition measured in the liver[60] or for efficient HCV internalization. This would a priori indicate that the deprotonated species of the compound **FOMe** examined in this report is seemingly not the relevant species to explain the antiviral activities reported. However, we showed that the anti-HCV activity of ladanein is strongly dependent on the pH (Figure 12A) at which it has been preincubated. This would suggest that high pH, among other factors (vide infra), favors bioactivation of ladanein. In addition to their acido-basic properties, the Fe(III) complexation of ladanein has then to be taken into consideration. The influence of a powerful Fe(III) chelator, ferrioxamine B (DFO), was examined. The antiviral activity of ladanein was found to be entirely abolished following the addition of an equimolar amount of the exogenous Fe(III) chelator (Figure 12B). This confirms that the antiviral activity of ladanein is Fe(III) and pH dependent. By mechanisms that have been not yet been identified, the flavone likely alters the physicochemical properties of the viral particles and inhibits their infectivity.

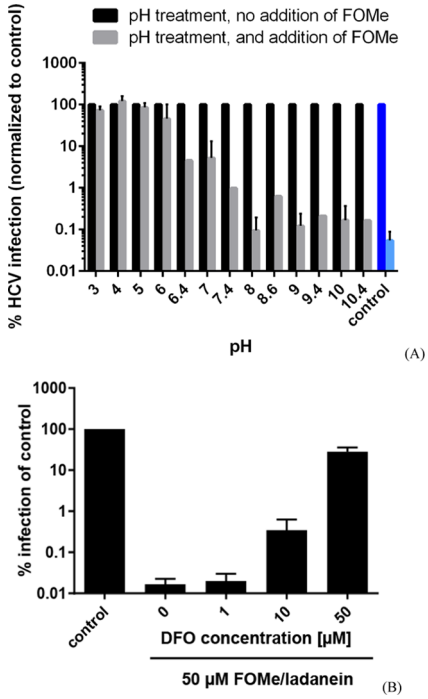

Figure 12. Percent of HCV infection as a function of pH in the presence or absence of **FOMe**/ladanein (A) and influence of iron chelator DFO on antiviral activity of **FOMe**/ladanein (B). (A) Ladanein-inhibiting HCV entry is strongly pH-dependent. Ladanein (concentration 50 μM) or solvent control was incubated with aqueous buffer at the indicated pH value for 10 min at room temperature (RT) prior to the addition of Jc1 reporter virus. Then, Lunet CD81 high cells were inoculated with the compound/virus mixture for 4 h at 37 °C, washed once with phosphate-buffered saline, and lysed 72 h after infection. Control infections where virus particles were treated with the given pH buffers without addition of compound were conducted in parallel. The HCV infection efficiency was determined by luciferase expression and is expressed relative to the infection experiments in absence of inhibitor at the respective pH. Mean values of one to three experiments are shown. The blue bars depict an HCV infection without pH modification (dark blue: solvent control, light blue: addition of **FOMe**). (B) HCV reporter virus (FF-Luc-Jc1) was preincubated for 15 min with indicated concentrations of the iron chelator DFO prior to the addition of a fixed concentration of the inhibitor and infection of Huh-7.5 human hepatoma cells. Seventy-two hours post infection, the cells were lysed and the firefly reporter activity was analyzed using a plate luminometer. Percent infection of solvent-treated control is given. Mean and SD of three independent experiments are given.

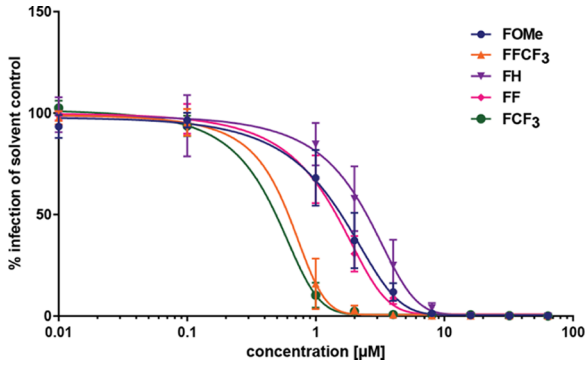

Figure 13. Luciferase reporter virus infection assay. Renilla luciferase virus (JcR-2a) was preincubated for 60 min at 37 °C with indicated concentrations of compounds prior to inoculation of Huh-7.5 human hepatoma cell lines. Cells were lysed 72 h p.i., and luciferase activity was measured. Mean values of four independent experiments and SD are given. The dose−response relationship (nonlinear regression) was analyzed using GraphPad Prism6 software.

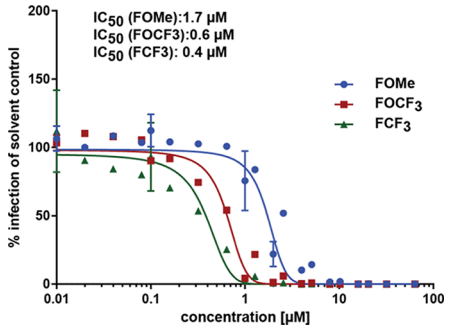

Figure 14. Luciferase infection assay. Huh-7.5 human hepatoma cells were inoculated with Renilla luciferase reporter virus (JcR-2a) in the presence of indicated concentration of compounds. Cells were lysed 72 h post infection, and luciferase activity was measured. For the different concentrations and compounds, mean values of one to three independent experiments and SD are given. The dose−response relationship was analyzed with GraphPad Prism6 software.

Structure−HCV Entry Inhibition Relationships. Inhibition of HCV entry was evaluated by inoculation of the highly permissive human hepatoma cell line Huh-7.5 with renilla luciferase reporter virus (JcR-2a).[61] Therefore, the virus was preincubated with the compounds for 60 min at 37 °C prior to inoculation of cells (Figure 13). Synthetic ladanein and the four analogues specifically inhibited HCV cell entry with an inhibitory concentration of 50% in the low micromolar range (Figure 14).

CONCLUSIONS

The physicochemical properties of ladanein **FOMe** and its analogues were thoroughly investigated in this study, and the resulting data were discussed with respect to other relevant biomolecules. This work was aimed at better understanding the reactivity and the MoA of this class of promising virucidal

DOI: 10.1021/acsomega.8b03332
ACS Omega 2019, 4, 4871−4887

compounds. Flavones might indeed be bioactivated by Fe(III)/pH to lead to C,C- and/or C,O-coupling products and particular attention to the effect of these two parameters on the virucidal activity was paid in this work. Last but not the least, scarce physicochemical data have been reported with respect to the metal complexation properties of these uncommon 5,6-hydroxylated flavones.

The pK_a values were attributed to the 6-OH unit. The substitution pattern on the B ring does not exert a significant role on the protonation properties of the A ring. Therefore, the substituent pattern of the B ring is seemingly not essential for fine-tuning the acido-basic properties of the flavone. It rather modulates the properties of the B (4-carbonyl unit) and C rings, making it possible to bring structural diversity in the B cycle.

The electrochemical behavior of these flavones was then described. Within the −0.8/1.2 V potential range, the flavones undergo a $2e^-$ irreversible oxidation and reduction mechanism that is limited by diffusion. This electrochemical behavior likely corresponds to an ECE process centered on the 5-OH and 6-OH groups borne by A cycle. From −2.35 to −1.5 V, a $1e^-$ (quasi)reversible process was evidenced and attributed to a redox process centered on the enone moiety of C cycle. In that case, substitution in B cycle exerted a marked influence on the redox properties. When examined within the full potential range (i.e., −2.35/1.2 V), side reactions (e.g., dismutation, coupling, etc.) likely occurred and led to new and still unidentified species that are characterized by the appearance of new peaks.

Ladanein **FOMe** and its analogues were also demonstrated to lead to the formation of ferric monochelates. Particular attention was herein paid to the Fe(III) complexation properties of ladanein and its analogues under physiological conditions. To avoid insoluble ferric species, **NTA** was used as an exogenous ligand. At pH 7.4, it was found that ternary flavone·Fe**NTA** complexes are formed. The stoichiometry of the complexes was further confirmed by ESI-MS. Last but not the least, involvement of the exogenous **NTA** ligand in the flavone−Fe(III) complexes prevented the flavone oxidation/degradation, likely due to alteration of the redox properties of the metallic center.

In the last approach, the Fe(III) uptake kinetics was investigated using stopped-flow spectrophotometry. Under acidic conditions, a first-order kinetics with respect to ladanein was observed. Over a much longer time span, ladanein oxidation triggered by Fe(III) complexation was observed in the form of a slow biphasic kinetic process that was not further investigated herein. The ferric flavone complexes are formed through two reaction routes involving either Fe^{3+} or $Fe(OH)^{2+}$. At pH 7.4, the complexation kinetics of Fe**NTA** by ladanein and some of its analogues was rationalized by the formation of a first kinetic intermediate that rapidly rearranges to the final ferric complex. With respect to the first rate-limiting step, comparable bimolecular rate constants were measured as a result of a process being controlled by the reactivity of $[Fe\mathbf{NTA}(OH)]^{2-}$. The second step was proposed to strongly depend on the nature of the bound flavone.

With respect to the antiviral activity, substitution by fluorinated groups allowed improving significantly the anti-infectious activity of the ladanein flavone. Combining a strong iron chelator such as DFO led to the abolishment of the ladanein antiviral activity. Indeed, preincubation for 15 min of the HCV reporter virus (FF-Luc-Jc1) with DFO prior to addition of ladanein and infection of Huh-7.5 human hepatoma cells led to full abolishment of the antiviral activity upon addition of an equimolar amount of the exogenous chelator with respect to ladanein. This clearly indicates that iron complexation by ladanein and its analogues is an essential prerequisite to their antiviral properties and further substantiates the nature and stoichiometry of the ferric complexes assessed under quasiphysiological conditions. On the other hand, a clear impact of the pH was demonstrated on the anti-HCV activity of ladanein above pH 6−7. Control experiments conducted in parallel with virus particles and aqueous buffers from pH 3 to 10.4 in the absence of the flavone confirm the specific HCV entry inhibition effect of ladanein above pH 6.

Altogether, these physicochemical parameters allowed getting a deeper insight into the reactivity and iron(III) coordination properties of ladanein and several bioactive analogues. Cross-analysis of the physicochemical and biological data allowed demonstrating that iron coordination by the flavone is a key step of the bioactivation responsible for the anti-HCV activity observed for ladanein. The preparation of a homogenous series of compounds highlighted the key structural features that are essential for the antiviral properties of these flavones. This extensive study paves the way for further development and improvement of this promising class of antiviral drug candidates.

EXPERIMENTAL METHODS

Chemical Synthesis. Starting materials were purchased from ABCR, GmbH & Co. KG, Sigma-Aldrich, Alfa Aesar, and Apollo Scientific and used as received. Solvents were purchased from Sigma-Aldrich and Carlo Erba. Reagent grade solvents were used for reactions and column chromatography, and analytical grade solvents were used for recrystallization. Dichloromethane (DCM) was distilled over CaH_2 under argon (Ar). Tetrahydrofuran (THF) was dried by using an activated alumina column under Ar. ^{1}H NMR spectra were recorded on Bruker AC 300 (300 MHz) with solvent peaks as reference. Chemical shifts (δ) are reported in parts per million. Multiplicities are given as: singlet (s), doublet (d), triplet (t), quartet (q), doublet of doublets (dd), multiplet (m), and broad singlet (br s). ^{13}C NMR spectra were recorded on Bruker AC 300 (75 MHz). Infrared (IR) spectra (cm^{-1}) were recorded neatly on a PerkinElmer Spectrum One Spectrophotometer. ESI high-resolution mass spectra were recorded on a Bruker micrOTOF spectrometer. Melting points were measured on a Stuart Melting Point 10 apparatus and are given uncorrected. Ladanein **FOMe** and its precursor **FPOMe** were synthesized according to reported procedures[6] (Scheme S1). Because many drawbacks were raised in the former synthesis (route A, Scheme S1), a more efficient, robust, and multigram synthesis (route B, Scheme S1) was developed to prepare ladanein and other analogues (Scheme S1). The synthesis of new ladanein precursors and analogues followed the same procedures (Scheme S1) and are described below. Routes A and B differed from the commercial starting materials, i.e., 4,6-dimethoxy-2-hydroxy acetophenone in route A and 2,6-dimethoxy-1,4-benzoquinone in route B. Both starting materials were used to produce the same acetophenone intermediate 2 but with different yields (35 vs 70% (+30% as its acetyl analogue 3) yield in routes A and B, respectively).

General Procedure for the Synthesis of the Final Precursors 4a−f (Scheme S1). A solution of LiHMDS was

DOI: 10.1021/acsomega.8b03332
ACS Omega 2019, 4, 4871−4887

prepared by adding *n*-BuLi (1.6 M in hexane, 7.5 equiv) to a solution of freshly distilled HMDS (7.9 equiv) in dry THF at 0 °C and stirred for 30 min. It was then added drop wise to a mixture of starting acetophenones **2** and **3**[6] (or separated and purified **2** or **3**) in dry THF under Ar at −78 °C. The mixture was stirred for 1 h at −78 °C, 2 h at −10 °C, and cooled down again to −78 °C. A solution of the benzoyl chloride (2 equiv) prepared in dry THF was added, and the reaction was stirred for 1 h at −78 °C and then at RT overnight. The solution was then poured into a mixture of crushed ice and concentrated HCl, extracted three times with DCM, and dried over $MgSO_4$. The solvent was removed under reduced pressure to yield a brown solid that was used without further purification. The crude product was then dissolved in acetic acid, and H_2SO_4 was added. The mixture was then stirred at 95 °C for 3.5−6 h. The solvent was evaporated under reduced pressure, water was added, and the aqueous phase was extracted three times with DCM. The organic phase was dried over $MgSO_4$, and the solvent was evaporated under reduced pressure to yield a dark brown solid. The crude product was dissolved in THF, and MeOH solution of LiOH in excess was added. The reaction mixture was stirred at RT for 2 h. The solution was then poured into water, and acetic acid was used to fix the pH at about 5. The aqueous phase was extracted three times with DCM, and the organic phase was thoroughly washed with NaOH solution (0.5 M). The aqueous phase was then acidified to neutral pH with HCl solution (1 M), and the aqueous phase was extracted three times with DCM. The solvent was evaporated under reduced pressure and the solid was recrystallized from water/EtOAc to lead to the pure targeted final precursor. The final precursors **4a−f** have been fully characterized (see the Supporting Information).

General Procedure for the Synthesis of Deprotected Flavones. Route A: A solution of the starting material (0.15 mmol, 1.0 equiv) in dry CH_2Cl_2 (5.0 mL) was stirred for 30 min at 0 °C. The BBr_3 solution (0.75 mL 1 M solution in CH_2Cl_2, 0.75 mmol, 5.0 equiv) was added drop wise at 0 °C, and the mixture was stirred for another 30 min. The MeOH (2.0 mL) was introduced for quenching the reaction, and saturated NaCl (10.0 mL) was added. The water layer was extracted with dichloromethane (3 × 50.0 mL) and diethyl ether (2 × 50.0 mL), and the combined organic layers were dried ($MgSO_4$) and evaporated. The residue was purified by chromatography on Sephadex LH-20 (eluent: MeOH/CH_2Cl_2 1:1) and recrystallized.

Route B: To a solution of the final precursor (1 equiv) in CH_3CN was added $MgBr_2$ (3 equiv). The reaction mixture was stirred for 3 h at 80 °C and monitored by thin-layer chromatography using DCM/EtOAc 1:1 as eluent. After consumption of all starting material, HCl solution (0.5 M) was added and the aqueous phase was extracted three times with EtOAc. The organic phase was then washed three times with HCl solution (0.5 M) and one time with water and brine. The organic layer was dried over $MgSO_4$, concentrated under reduced pressure, and recrystallized from DCM to yield the targeted product. The deprotected flavones **FOMe**, **FH**, **FF**, **FCF_3**, **$FFCF_3$**, and **$FOCF_3$** have been fully characterized (see the Supporting Information).

X-ray Crystal Structures. *Natural Ladanein.* Yellow crystal (plate), dimensions 0.400 × 0.310 × 0.020 mm^3, crystal system monoclinic, space group $P2_1/c$, Z = 4, a = 7.1846(19) Å, b = 26.741(7) Å, c = 7.2404(19) Å, α = 90°, β = 92.287(6)°, γ = 90°, V = 1390.0(6) $Å^3$, ρ = 1.502 g cm^{-3}, T = 200(2) K, θ_{max} = 28.411°, radiation Mo Kα, λ = 0.71073 Å, 0.5° ω scans with a charge-coupled device (CCD) area detector, covering the asymmetric unit in reciprocal space with a mean redundancy of 4.13 and a completeness of 99.2% to a resolution of 0.79 Å, 14 338 reflections measured, 3469 unique (R(int) = 0.0436), 2818 observed ($I > 2\sigma(I)$), intensities corrected for Lorentz and polarization effects, empirical scaling and absorption correction applied using SADABS[62] based on the Laue symmetry of the reciprocal space, μ = 0.12 mm^{-1}, T_{min} = 0.75, T_{max} = 0.98, structure solved with Bruker SHELXTL[63] and refined against F^2 with a full-matrix least-squares algorithm using the SHELXL software,[64] 218 parameters refined, hydrogen atoms treated using appropriate riding models, except of those at heteroatoms, which were refined isotropically, goodness of fit 1.30 for observed reflections; final residual values $R_1(F)$ = 0.092, w$R(F^2)$ = 0.169 for observed reflections, residual electron density −0.32 to 0.44 e $Å^{-3}$.

Synthetic Ladanein FOMe. Yellow crystal (plate), dimensions 0.200 × 0.140 × 0.060 mm^3, crystal system triclinic, space group $P\bar{1}$, Z = 2, a = 6.8268(10) Å, b = 7.6728(11) Å, c = 15.650(2) Å, α = 83.681(3)°, β = 85.254(3)°, γ = 86.152(3)°, V = 810.6(2) $Å^3$, ρ = 1.419 g cm^{-3}, T = 274(2) K, θ_{max} = 28.337°, radiation Mo Kα, λ = 0.71073 Å, 0.5° ω scans with a CCD area detector, covering the asymmetric unit in reciprocal space with a mean redundancy of 2.13 and a completeness of 98.8% to a resolution of 0.77 Å, 8504 reflections measured, 3986 unique (R(int) = 0.0265), 2852 observed ($I > 2\sigma(I)$), intensities corrected for Lorentz and polarization effects, empirical scaling and absorption correction applied using SADABS[62] based on the Laue symmetry of the reciprocal space, μ = 0.11 mm^{-1}, T_{min} = 0.92, T_{max} = 0.98, structure solved with Bruker SHELXTL[63] and refined against F^2 with a full-matrix least-square algorithm using the SHELXL software,[64] 241 parameters refined, hydrogen atoms treated using appropriate riding models, except of those at heteroatoms, which were refined isotropically, goodness of fit 1.14 for observed reflections, final residual values $R_1(F)$ = 0.077, w$R(F^2)$ = 0.162 for observed reflections, residual electron density −0.30 to 0.35 e $Å^{-3}$.

Final Precursor FPOMe. Yellowish crystal (polyhedron), dimensions 0.390 × 0.080 × 0.060 mm^3, crystal system orthorhombic, space group *Pbca*, Z = 8, a = 14.659(2) Å, b = 9.8378(11) Å, c = 21.236(2) Å, α = 90°, β = 90°, γ = 90°, V = 3062.5(6) $Å^3$, ρ = 1.424 g cm^{-3}, T = 200(2) K, θ_{max} = 25.005°, radiation Mo Kα, λ = 0.71073 Å, 0.5° ω scans with a CCD area detector, covering the asymmetric unit in reciprocal space with a mean redundancy of 1.95 and a completeness of 98.4% to a resolution of 0.84 Å, 5200 reflections measured, 2657 unique (R(int) = 0.0679), 1308 observed ($I > 2\sigma(I)$), intensities corrected for Lorentz and polarization effects, empirical scaling and absorption correction applied using SADABS[62] based on the Laue symmetry of the reciprocal space, μ = 0.11 mm^{-1}, T_{min} = 0.91, T_{max} = 1.00, structure solved with Bruker SHELXTL[63] and refined against F^2 with a full-matrix least-square algorithm using the SHELXL software,[64] 224 parameters refined, hydrogen atoms treated using appropriate riding models, except of those at heteroatoms, which were refined isotropically, goodness of fit 0.94 for observed reflections, final residual values $R_1(F)$ = 0.050, w$R(F^2)$ = 0.082 for observed reflections, residual electron density −0.26 to 0.24 e $Å^{-3}$.

DOI: 10.1021/acsomega.8b03332
ACS Omega 2019, 4, 4871−4887

Physicochemical Investigations. *Solvents and Materials.* Distilled water was purified by passing it through a bed of activated carbon (Bioblock Scientific ORC-83005) and ion exchanger (Bioblock Scientific R3-83002, M3-83006). Methanol (Merck, p.a.) of spectrophotometric grade and water were deoxygenated by CO_2- and O_2-free Ar (Sigma Oxiclear cartridge). The electrochemical experiments were conducted in spectroscopic grade DMSO (BioReagent for molecular biology, >99.9%, Sigma) at room temperature (25 ± 1 °C) containing 0.1 M of *n*-Bu_4PF_6 as the inert supporting electrolyte.[65] The stock solutions were prepared by weighting solid products (Mettler Toledo XA105 Dual Range (0.01/0.1 mg to 41/120 g)). Dissolution of the ligands was achieved by using an ultrasonic bath (Bandelin Sonorex RK102). For the determination of the acido-basic properties, the ionic strength was maintained at 0.1 M with *n*-tetrabutylammonium perchlorate (NEt_4ClO_4, Fluka, puriss) and the measurements were carried out at 25.0(2) °C.

CAUTION! Perchlorate salts combined with organic ligands are potentially explosive and must be handled with great care.[66]

Fe(III) perchlorate stock solutions (Fluka) were prepared in water under acidic conditions (pH < 1.5) immediately before use, and their concentrations were determined by using UV−vis absorption (ε^{240} = 4.16 × 10^3 M^{-1} cm^{-1} and ε^{260} = 2.88 × 10^3 M^{-1} cm^{-1}).[67]

The Fe**NTA** solutions were prepared freshly by adding an iron(III) aqueous solution (1 equiv) to 1 equiv of solid **NTA** ($C_6H_9NO_6$, Fluka, purum). Few drops of $HClO_4$ (70%) were added. The pH of the mixture was then raised to 7.4 with a HEPES buffer (0.1 M). A slight excess of **NTA** with respect to iron(III) was always used to ensure complete complexation of iron(III) and avoid free ferric species.

Spectrophotometric Titrations of the Flavones vs pH. First, stock solutions of the flavones were prepared by quantitative dissolution of the corresponding solid samples in methanol. For solubility reasons, the flavones were then diluted in CH_3OH/H_2O solvent (80/20 w/w) containing the supporting electrolyte (0.1 M NEt_4ClO_4, Fluka, puriss). Forty millimeters of the solution were then introduced into a jacketed cell (Metrohm) maintained at 25.0(2) °C (Lauda E200 thermostat) under Ar atmosphere. The free hydrogen-ion concentration was measured with a combined glass electrode (Metrohm 6.0234.500, Long Life; Ag/AgCl reference; NaCl 0.1 M (Fluka, p.a.)) and an automatic titrator system 794 Basic Titrino (Metrohm; Tiamo light 1.2 program for the acquisition of the potentiometric data). The glass electrode was calibrated by titrating known amounts of $HClO_4$ (~7 × 10^{-2} M from $HClO_4$, Prolabo, normapur, 70% min) with CO_2-free NEt_4OH solution (~7 × 10^{-2} M from NEt_4OH ~40% in water; Aldrich, purum) in CH_3OH/H_2O solvent.[68] The $HClO_4$ and NEt_4OH solutions were prepared just before use and titrated with sodium tetraborate ($B_4Na_2O_7{\cdot}10H_2O$, Fluka, puriss, p.a.) and potassium hydrogen phthalate ($C_8H_5KO_3$, Fluka, puriss, p.a.), respectively, using methyl orange (RAL) and phenolphthalein (Prolabo, purum) indicators. The flavone solution was acidified, and the absorption titration (2 < pH < 12) was then carried out by addition of known volumes of the base. Special care was taken to ensure that complete equilibration was attained. Absorption spectra were recorded with a Varian Cary 50 spectrophotometer fitted with Hellma optical fibers (Hellma, 041.002-UV) and an immersion probe (l = 1 cm) made of quartz suprazil (Hellma, 661.500-QX).

Spectrophotometric Titrations of Ladanein and Its Analogues with Fe(III) at pH 2.0. Stock solutions of the flavones were prepared in CH_3OH/H_2O (80/20 w/w) containing a supporting electrolyte (0.1 M NEt_4ClO_4, Fluka, puriss) and then freshly diluted with $HClO_4$ (10^{-2} M) to lead to a final concentration of ~5.92 × 10^{-5} and ~4−7 × 10^{-5} M for **FOMe** and the other flavones, respectively. Microvolumes of a concentrated Fe(III) solution that were prepared just before use were added to an aliquot of 0.5 mL (or 2.5 mL) of the flavone solution in a quartz optical cell (Hellma, l = 1 cm). The $[Fe(III)]_0/[flavone]_0$ ratio was varied from 0 to ~1.2−1.6, and after each addition, precautions have been taken to ensure that the complete equilibration was achieved. The UV−vis spectra were then recorded from 230 to 800 nm on a Cary 50 (Varian) or 300 (Varian) spectrophotometer maintained at 25.0(2) °C (Lauda E200 thermostat).

Spectrophotometric Titrations of Ladanein and Its Analogues with Fe(III) at pH 7.4 in the Presence of an Exogenous NTA Ligand. **NTA** was used to characterize and quantify the corresponding ladanein ferric complexes at physiological pH.[53−56] A stock solution of ladanein (5.41 × 10^{-5} M) was prepared in HEPES buffer at pH 7.4 (0.1 M in CH_3OH/H_2O, 80/20 w/w). The ionic strength was adjusted to 0.1 M with NEt_4ClO_4 (Fluka, puriss). Microvolumes of a concentrated Fe**NTA** solution (2.41 × 10^{-3} M) were added to an aliquot of 2 mL of the flavone solution disposed in a quartz optical cell (Hellma, l = 1 cm). Along the absorption, the $[FeNTA]_0/[ladanein]_0$ ratio was varied from 0 to 2.0. After each addition, the solution was mixed and care was taken to ensure complete equilibration. The UV−vis spectra were recorded on a Cary 300 (Varian) spectrophotometer maintained at 25.0(2) °C (Lauda E200 thermostat).

Analysis and Processing of the Spectroscopic Data. The spectrophotometric data were analyzed with Specfit[69] program that adjusts the absorptivities and the stability constants of the species formed at equilibrium. Specfit uses factor analysis to reduce the absorbance matrix and to extract the eigenvalues prior to the multiwavelength fit of the reduced data set according to the Marquardt algorithm.[70,71]

Electrochemistry. The redox properties of ladanein and its analogues were investigated by cyclic voltammetry (CV) in DMSO solvent containing 0.1 M *n*-Bu_4PF_6. DMSO was found to be a suitable solvent[72−74] to characterize the electrochemical properties of our flavones (i.e., potential limits from +0.9 to −3.9 V versus Fc/Fc^+, E = +0.524 V/Ag/AgCl[73]). CVs of ladanein **FOMe** and its analogues (~mM) were recorded with a VoltaLab 50 potentiostat/galvanostat equipment (Radiometer Analytical; MDE15 polarographic stand; PST050 analytical voltammetry; CTV101 speed control unit) controlled by the VoltaMaster 4 electrochemical software. A conventional three-electrode cell (10 mL) fitted with a glassy carbon (GC) disk (s = 0.07 cm^2) set into a Teflon rotating tube was used as the working electrode, a Pt wire was used as a counterelectrode, and a KCl(3 M)/Ag/AgCl reference electrode (+210 mV vs normal hydrogen electrode) was employed.[75] Prior to any measurement, the GC electrode surface was carefully polished with an aluminum oxide suspension (0.3 μm, Escil) disposed on a silicon carbide abrasive sheet (grit 800/2400). The flavone solution (ca. mM) was vigorously stirred in the electrochemical cell and purged with O_2-free (Sigma Oxiclear cartridge) Ar for 15 min before

DOI: 10.1021/acsomega.8b03332
ACS Omega 2019, 4, 4871−4887

the voltammetry experiment was initiated. An Ar atmosphere was maintained during the measurement procedure. The voltage sweep rate was varied from 50 mV s^{-1} to 6 V s^{-1}. Oxidation and reduction peak potentials were measured at a scan rate of 200 mV s^{-1} unless otherwise stated.

Kinetic Measurements. The formation kinetics was studied at 25.0(2) °C with a SX-18MV stopped-flow spectrophotometer (Applied Photophysics).

The formation kinetics of the ladanein ferric complexes was first studied under acidic conditions (5.88×10^{-3} M $\leq [H^+] \leq 9.4 \times 10^{-2}$ M) in excess of Fe(III) (5.54×10^{-3} M < [Fe(III)] < 5.54×10^{-4} M). At least 10 times more concentrated solution of Fe(III) with respect to ladanein was used to impose pseudo-first-order conditions. Ladanein concentration was fixed at ~$3-5 \times 10^{-5}$ M. The reaction was monitored at 650 nm (maximum of the LMCT absorption band).

The uptake kinetics of Fe(III) by ladanein **FOMe**, **FCF_3**, **$FFCF_3$**, or apigenin was also investigated at pH 7.4 (0.1 M HEPES buffer) in the presence of **NTA** used as an auxiliary iron(III) chelator. The experiments were performed in excess of the flavones with a ratio [Fe(III)]/[**NTA**] ~ 1 ($[Fe\mathbf{NTA}]_0 = 2.3 \times 10^{-5}$ M). At least 10 times more concentrated solutions of the flavones with respect to Fe(**NTA**) were used to impose pseudo-first-order conditions. The uptake kinetics was recorded at the maximum of the LMCT absorption band (Table 6).

Analysis and Processing of the Kinetic Data. The data sets, averaged out of at least three replicates, were analyzed with the commercial software Biokine.[76] This program fits up to three exponential functions to the experimental curves with the Simplex algorithm[77] after initialization with a Padé–Laplace method.[78]

■ ASSOCIATED CONTENT

Supporting Information

The Supporting Information is available free of charge on the ACS Publications website at DOI: 10.1021/acsomega.8b03332.

> Experimental sections, figures, tables and schemes; chemical analysis data of the newly synthesized flavones; X-ray structural data of ladanein **FOMe** and its final precursor **FPOMe**; absorption vs pH titrations of the flavones; electrochemical data (CV) of the free flavones in DMSO; absorption titrations of the flavones as a function of Fe(III) (or Fe**NTA**) at pH 2 (or at pH 7.4); Fe(III) uptake kinetics of ladanein under acidic conditions; Fe**NTA** uptake kinetics of ladanein and some of its analogues at pH 7.4; HCV entry inhibition studies; CCDC 1876096 (**FPOMe**), 1876097 (**FOMe** natural), and 1876098 (**FOMe** synthetic) (PDF)

■ AUTHOR INFORMATION

Corresponding Authors

*E-mail: elisabeth.davioud@unistra.fr (E.D.-C.).
*E-mail: elhabiri@unistra.fr (M.E.).

ORCID

Elisabeth Davioud-Charvet: 0000-0001-7026-4034
Mourad Elhabiri: 0000-0001-6371-7533

Notes

The authors declare no competing financial interest.

■ ACKNOWLEDGMENTS

E.D.-C. thanks Beate Jannack from Biochemie-Zentrum Heidelberg for the production of the first batches of synthetic ladanein and both fluorinated flavones **FCF_3** and **$FOCF_3$**. The ungraduated students, Palazzi Paul, Mehmeti Iris, and Meziere Marie are acknowledged for their participation in the physicochemical properties of flavones. This work was made possible by the grant of the Laboratoire d'Excellence ParaFrap (grant LabEx ParaFrap ANR-11-LABX-0024 to E.D.-C.). The Centre National de la Recherche Scientifique (CNRS France, to E.D.-C. and M.E.), University of Strasbourg, partly supported this work. X.M.-B. is grateful to Strasbourg University for his doctoral fellowship (MRT) from the research Ministry for Research. B. Mießen from Helmholtz Centre for Infection Research, Braunschweig, Germany is acknowledged for the picture of HCV virion used in the table of content for presenting the article.

■ REFERENCES

(1) Mouradov, A.; Spangenberg, G. Flavonoids: a metabolic network mediating plants adaptation to their real estate. *Front. Plant Sci.* **2014**, *5*, 620.

(2) Geuenich, S.; Goffinet, C.; Venzke, S.; Nolkemper, S.; Baumann, I.; Plinkert, P.; Reichling, J.; Keppler, O. T. Aqueous extracts from peppermint, sage and lemon balm leaves display potent anti-HIV-1 activity by increasing the virion density. *Retrovirology* **2008**, *5*, 27.

(3) Pietschmann, T.; Haid, S.; Gentzsch, J.; Grethe, C.; Davioud-Charvet, E.; Lanfranchi, D.-A.; Elhabiri, M.; Benlloch-Martin, X. Flavone Derivatives and Their Use. PCT International Application WO2013139487A1, 2013.

(4) Haid, S.; Novodomská, A.; Gentzsch, J.; Grethe, C.; Geuenich, S.; Bankwitz, D.; Chhatwal, P.; Jannack, B.; Hennebelle, T.; Bailleul, F.; Keppler, O. T.; Poenisch, M.; Bartenschlager, R.; Hernandez, C.; Lemasson, M.; Rosenberg, A. R.; Wong-Staal, F.; Davioud-Charvet, E.; Pietschmann, T. A plant-derived flavonoid inhibits entry of all HCV genotypes into human hepatocytes. *Gastroenterology* **2012**, *143*, 213.e3–222.e5.

(5) (a) Martin-Benlloch, X.; Novodomská, A.; Jacquemin, D.; Davioud-Charvet, E.; Elhabiri, M. Iron(III) coordination properties of ladanein, a flavone lead with a broad-spectrum antiviral activity. *New J. Chem.* **2018**, *42*, 8074–8087. (b) Martin-Benlloch, X. *Synthesis and Physico-chemical Study of a Novel Flavone Antiviral Lead*; Université de Strasbourg, 2015.

(6) Martin-Benlloch, X.; Elhabiri, M.; Lanfranchi, D. A.; Davioud-Charvet, E. A practical and economical high-yielding six steps-sequence synthesis of a flavone: application to the multigram scale synthesis of ladanein. *Org. Process Res. Dev.* **2014**, *18*, 613–617.

(7) (a) Sowa, M.; Slepokura, K.; Matczak-Jon, E. A 1:1 cocrystal of baicalein with nicotinamide. *Acta Crystallogr., Sect. C: Cryst. Struct. Commun.* **2012**, *68*, o262. (b) Hibbs, D. E.; Overgaard, J.; Gatti, C.; Hambley, T. W. The electron density in flavones I. Baicalein. *New J. Chem.* **2003**, *27*, 1392. (c) Rossi, M.; Meyer, R.; Constantinou, P.; Caruso, F.; Castelbuono, D.; O'Brien, M.; Narasimhan, V. Molecular structure and activity toward DNA of baicalein, a flavone constituent of the Asian herbal medicine "Sho-saiko-to". *J. Nat. Prod.* **2001**, *64*, 26.

(8) Sharma, D.; Gupta, V. K.; Brahmachari, G.; Mondal, S.; Gangopadhyay, A. X-ray study of weak interactions in two flavonoids. *Bull. Mater. Sci.* **2007**, *30*, 469.

(9) Mou, M.-Y.; Pi, K.; Zhang, Q.-L.; Zhang, Y.-Q.; Zhang, Q.-J. 5,7-Dihydroxy-6,4-dimethoxyflavone. *Acta Crystallogr., Sect. E: Struct. Rep. Online* **2008**, *64*, o71.

(10) Chou, N. H.-H.; Parvez, M.; Ali, M. S.; Ahmed, S.; Ahmed, W. Cirsimaritin. *Acta Crystallogr., Sect. E: Struct. Rep. Online* **2002**, *58*, o285–o287.

(11) Parvez, M.; Riaz, M.; Malik, A. Eupatorin. *Acta Crystallogr., Sect. E: Struct. Rep. Online* **2001**, *57*, o289–o291.

DOI: 10.1021/acsomega.8b03332
ACS Omega 2019, 4, 4871–4887

(12) Adizov, S. M.; Mukhamathanova, R. F.; Turgunov, K. K.; Sham'yanov, I. D.; Tashkhodjaev, B. 5,7-Dihydroxy-2-(3-hydroxy-4,5-dimethoxyphenyl)-6-methoxy-4*H*-chromen-4-one. *Acta Crystallogr., Sect. E: Struct. Rep. Online* **2013**, *69*, o578.
(13) Li, H.-J.; Zhou, D.-L.; Xu, T.-J.; Lam, C.-K.; Lan, W.-J. 5,6,7,5′-Tetramethoxy-3′,4′-methylene-dioxyflavone monohydrate. *Acta Crystallogr., Sect. E: Struct. Rep. Online* **2012**, *68*, o1390.
(14) Hall, B. J.; Hanrahan, J. R.; Johnston, G. A. R.; Hambley, T. W.; Hibbs, D. E. 6-Methylflavone. *Acta Crystallogr., Sect. E: Struct. Rep. Online* **2001**, *57*, o592 and references therein. .
(15) (a) Rossi, M.; Rickles, L. F.; Halpin, W. A. The crystal and molecular structure of quercetin: A biologically active and naturally occurring flavonoid. *Bioorg. Chem.* **1986**, *14*, 55. (b) Rossi, M.; Cantrell, J. S.; Farber, A. J.; Dyott, T.; Carrell, H. L.; Glusker, J. P. Molecular Structures of 5,6- and 7,8-Benzoflavones, Inhibitors of Aryl Hydrocarbon Hydroxylase. *Cancer Res.* **1980**, *40*, 2774.
(16) Wolniak, M.; Oszmianskib, J.; Wawera, I. Solid-state NMR studies and DFT calculations of flavonoids: baicalein, baicalin and wogonoside. *Magn. Reson. Chem.* **2008**, *46*, 215.
(17) Thompson, M.; Williams, G. R.; Elliot, G. E. P. Stability of flavonoid complexes of copper(II) and flavonoid antioxidant activity. *Anal. Chim. Acta* **1976**, *85*, 375.
(18) Murata, A.; Tominaga, M.; Inoue, H.; Suzuki, T. Complex formation of 5-hydroxyflavone and 5-hydroxyisoflavone with metallic ions and their solvent extraction. *Bunseki kagaku* **1973**, *22*, 179.
(19) Slabbert, N. P. Ionisation of some flavanols and dihydroflavonols. *Tetrahedron* **1977**, *33*, 821.
(20) Carrër, C. Chélation de métaux de transition par des polyphénols du régime alimentaire. Ph.D. Thesis, Université Louis Pasteur de Strasbourg, 2005.
(21) McDaniel, D. H.; Brown, H. C. An extended table of Hammett substitutent constants based on the ionization of substituted benzoic acids. *J. Org. Chem.* **1958**, *23*, 420.
(22) Hammett, L. P. The effect of structure upon the reactions of organic compounds. Benzene derivatives. *J. Am. Chem. Soc.* **1937**, *59*, 96.
(23) Hansch, C.; Leo, A.; Taft, R. W. A survey of Hammett substituent constants and resonance and field parameters. *Chem. Rev.* **1991**, *91*, 165.
(24) Salas-Reyes, M.; Hernández, J.; Domínguez, Z.; González, F. J.; Astudillo, P. D.; Navarro, R. E.; Martínez-Benavidez, E.; Velázquez-Contreras, C.; Cruz-Sánchez, S. Electrochemical oxidation of caffeic and ferulic acid derivatives in aprotic medium. *J. Braz. Chem. Soc.* **2011**, *22*, 693.
(25) Bard, A. J.; Faulkner, L. R. *Electrochemical Methods, Fundamentals and Applications*, 2nd ed.; John Wiley & Sons: New York, 2001; pp 236, 503, 709.
(26) Harrison, J. A.; Khan, Z. A. The oxidation of hydrazine on platinum in acid solution. *J. Electroanal. Chem. Interfacial Electrochem.* **1970**, *28*, 131.
(27) Petrucci, R.; Astolfi, P.; Greci, L.; Firuzi, O.; Saso, L.; Marrosu, G. A spectroelectrochemical and chemical study on oxidation of hydroxycinnamic acids in aprotic medium. *Electrochim. Acta* **2007**, *52*, 2461.
(28) Nicholson, R. S.; Shain, I. Theory of stationary electrode polarography. Single scan and cyclic methods applied to reversible, irreversible, and kinetic systems. *Anal. Chem.* **1964**, *36*, 706.
(29) Andrieux, C. P.; Saveant, J. M. Heterogeneous (chemically modified electrodes, polymer electrodes) vs. homogeneous catalysis of electrochemical reactions. *J. Electroanal. Chem. Interfacial Electrochem.* **1978**, *93*, 163.
(30) Guidelli, R.; Compton, R. G.; Feliu-Martinez, J. M.; Gileadi, E.; Lipkowski, J.; Schmickler, W.; Trasatti, S. *Definition of the Transfer Coefficient*; IUPAC, 2013.
(31) Bard, A. J.; Faulkner, R. *Electrochemical Methods*; John Wiley: New York, 1980.
(32) (a) Vakulskaya, T. I.; Larina, L. I.; Vashchenko, A. V. Radical anions of flavonoids. *Magn. Reson. Chem.* **2011**, *49*, 508. (b) Senboku, H.; Yamauchi, Y.; Kobayashi, N.; Fukui, A.; Hara, S. Some mechanistic studies on electrochemical carboxylation of flavones to yield flavanone-2-carboxylic acids. *Electrochim. Acta* **2012**, *82*, 450.
(33) Nagarajan, P.; Sulochana, N.; Muralidharan, V. S. Cyclic voltammetric reduction of 7-hydroxy and acetoxy flavones at glassy carbon electrode. *Bull. Electrochem.* **2004**, *20*, 93.
(34) (a) Nakayama, T.; Shimizu, T.; Torii, Y.; Miki, S.; Hamanoue, K. A comparison of the photochemistry of flavanone with that of flavone originating from their lowest excited triplet states in ethanol. *J. Photochem. Photobiol., A* **1997**, *111*, 35. (b) Kawata, H.; Kumagai, T.; Suzuki, E.; Niizuma, S. Photoreduction of flavone: identification of the photoproducts and reaction mechanism. *J. Photochem. Photobiol., A* **1996**, *101*, 201.
(35) (a) Chen, A.-W.; Kuo, W.-B.; Chen, C.-W. Photochemical Synthesis of 2,2′-Biflavanones from Flavone. *J. Chin. Chem. Soc.* **2003**, *50*, 123. (b) Handy, S. T.; Omune, D. A chelation effect on the pathway between intramolecular hydrodimerization and pinacol coupling. *Org. Lett.* **2005**, *7*, 1553. (c) Berthelot, J.; Guette, C.; Fournier, F.; Davoust, D. Electro-hydrodimerisation d'enones en presence de sels metalliques. *Tetrahedron Lett.* **1987**, *28*, 1881.
(36) Elhabiri, M.; Carrër, C.; Marmolle, F.; Traboulsi, H. Complexation of iron(III) by catecholate-type polyphenols. *Inorg. Chim. Acta* **2007**, *360*, 353−359.
(37) (a) Brandel, J.; Humbert, N.; Elhabiri, M.; Schalk, I. J.; Mislin, G. L. A.; Albrecht-Gary, A. M. Role of pyochelin in *Pseudomonas aeruginosa*: a physico-chemical characterization of the iron(III), copper(II) and zinc(II) complexes. *Dalton Trans.* **2012**, *41*, 2820. (b) Flynn, C. M., Jr. Hydrolysis of inorganic iron(III) salts. *Chem. Rev.* **1984**, *84*, 31.
(38) Fernandez, M. T.; Mira, L. M.; Florêncio, M. H.; Jennings, K. R. Iron and copper chelation by flavonoids: an electrospray mass spectrometry study. *J. Inorg. Biochem.* **2002**, *92*, 105.
(39) Grant, M.; Jordan, R. B. Kinetics of solvent water exchange on iron(III). *Inorg. Chem.* **1981**, *20*, 55.
(40) (a) Helm, L.; Merbach, A. E. Inorganic and bioinorganic solvent exchange mechanisms. *Chem. Rev.* **2005**, *105*, 1923. (b) Richens, D. T. Ligand substitution reactions at inorganic centers. *Chem. Rev.* **2005**, *105*, 1961.
(41) Albrecht-Gary, A. M.; Crumbliss, A. L. In *Metal Ions in Biological Systems*; Sigel, A., Sigel, H., Eds.; Marcel Dekker, Inc.: New York, 1998; Vol. *35*, p 239.
(42) Crumbliss, A. L.; Albrecht-Gary, A. M. *Scientific Bridges for 2000 and Beyond*; Académie des Sciences, Institut de France: Paris, 1999; pp 73−89.
(43) Biruš, M.; Bradič, Z.; Krznarić, G.; Kujundžic, N.; Pribanić, M.; Wilkins, P. C.; Wilkins, R. G. Kinetics of stepwise hydrolysis of ferrioxamine B and of formation of diferrioxamine B in acid perchlorate solution. *Inorg. Chem.* **1987**, *26*, 1000.
(44) Batinic-Haberle, I.; Biruš, M.; Pribanic, M. Siderophore chemistry of vanadium. Kinetics and equilibrium of interaction between vanadium(IV) and desferrioxamine B in aqueous acidic solutions. *Inorg. Chem.* **1991**, *30*, 4882.
(45) Albrecht-Gary, A. M.; Blanc, S.; Rochel, N.; Ocaktan, A. Z.; Abdallah, M. A. Bacterial iron transport: coordination properties of pyoverdin PaA, a peptidic siderophore of *Pseudomonas aeruginosa*. *Inorg. Chem.* **1994**, *33*, 6391.
(46) (a) Hynes, M. J.; O'Coinceanainn, M. The kinetics and mechanisms of the reaction of iron(III) with gallic acid, gallic acid methyl ester and catechin. *J. Inorg. Biochem.* **2001**, *85*, 131. (b) Hynes, M. J.; O'Coinceanainn, M. The kinetics and mechanisms of reactions of iron(III) with caffeic acid, chlorogenic acid, sinapic acid, ferulic acid and naringin. *J. Inorg. Biochem.* **2004**, *98*, 1457.
(47) Mentasti, E.; Pelizzetti, E. Reactions between iron(III) and catechol (o-dihydroxybenzene). part I. Equilibria and kinetics of complex formation in aqueous acid solution. *J. Chem. Soc., Dalton Trans.* **1973**, 2605.
(48) Cavasino, F. P.; Di Dio, E. Kinetic investigation of formation and dissociation of iron(III) monophenolate complexes. *J. Chem. Soc. A* **1970**, 1151.

DOI: 10.1021/acsomega.8b03332
ACS Omega 2019, 4, 4871−4887

(49) Zhang, Z.; Jordan, R. B. Kinetics of Dissociation of Iron(III) Complexes of Tiron in Aqueous Acid. *Inorg. Chem.* **1996**, *35*, 1571.
(50) Xu, J.; Jordan, R. B. Equilibrium and kinetic studies of the complexing of iron(III) by 1,2-dihydroxybenzene derivatives. *Inorg. Chem.* **1988**, *27*, 1502.
(51) Gabričević, M.; Crumbliss, A. L. Kinetics and mechanism of iron(III)−nitrilotriacetate complex reactions with phosphate and acetohydroxamic Acid. *Inorg. Chem.* **2003**, *42*, 4098.
(52) Biruš, M.; Kujundžić, N.; Pribanić, M. The reactivity of different iron(III) species in the formation of monoacethydroxamatoiron(III) complex. *Inorg. Chim. Acta* **1981**, *55*, 65.
(53) Bates, G. W.; Billups, C.; Saltman, P. The kinetics and mechanism of iron(III) exchange between chelates and transferrin. I. The complexes of citrate and nitrilotriacetic acid. *J. Biol. Chem.* **1967**, *242*, 2810.
(54) Li, Y.; Harris, W. R.; Maxwell, A.; McGillivray, R. T. A.; Brown, T. Kinetic studies on the removal of iron and aluminum from recombinant and site-directed mutant N-lobe half transferrins. *Biochemistry* **1998**, *37*, 14157.
(55) Chahine, J. M. E. H.; Pakdaman, R. Transferrin, a mechanism for the holoprotein formation from nitrilotriacetato-Fe(III)-transferrin mixed complex. *J. Chim. Phys.* **1996**, *93*, 283.
(56) Gabričević, M.; Anderson, D. S.; Mietzner, T. A.; Crumbliss, A. L. Kinetics and mechanism of iron(III) complexation by ferric binding protein: The role of phosphate. *Biochemistry* **2004**, *43*, 5811.
(57) Faller, B.; Nick, H. Kinetics and mechanism of iron(III) removal from citrate by desferrioxamine B and 3-hydroxy-1,2-dimethyl-4-pyridone. *J. Am. Chem. Soc.* **1994**, *116*, 3860.
(58) Nowack, B. Environmental chemistry of aminopolycarboxylate chelating agents. *Environ. Sci. Technol.* **2002**, *36*, 4009.
(59) Sanchiz, J.; Esparza, P.; Dominguez, S.; Brito, F.; Mederos, A. Solution studies of complexes of iron(III) with iminodiacetic, alkyl-substituted iminodiacetic and nitrilotriacetic acids by potentiometry and cyclic voltammetry. *Inorg. Chim. Acta* **1999**, *291*, 158.
(60) Aoi, W.; Marunaka, Y. Importance of pH homeostasis in metabolic health and diseases: crucial role of membrane proton transport. *BioMed. Res. Int.* **2014**, *2014*, No. 598986.
(61) Reiss, S.; Rebhan, I.; Backes, P.; Romero-Brey, I.; Erfle, H.; Matula, P.; Kaderali, L.; Poenisch, M.; Blankenburg, H.; Hiet, M. S.; Longerich, T.; Diehl, S.; Ramirez, F.; Balla, T.; Rohr, K.; Kaul, A.; Bühler, S.; Pepperkok, R.; Lengauer, T.; Albrecht, M.; Eils, R.; Schirmacher, P.; Lohmann, V.; Bartenschlager, R. Recruitment and activation of a lipid kinase by hepatitis C virus NS5A is essential for integrity of the membranous replication compartment. *Cell Host Microbe* **2011**, *9*, 32.
(62) Krause, L.; Herbst-Irmer, R.; Sheldrick, G. M.; Stalke, D. Comparison of silver and molybdenum microfocus X-ray sources for single-crystal structure determination. *J. Appl. Crystallogr.* **2015**, *48*, 3−10.
(63) Sheldrick, G. M. SHELXT − Integrated space-group and crystal-structure determination. *Acta Crystallogr., Sect. A: Found. Adv.* **2015**, *71*, 3−8.
(64) Sheldrick, G. M. Crystal structure refinement with SHELXL. *Acta Crystallogr., Sect. C: Struct. Chem.* **2015**, *71*, 3−8.
(65) Izutsu, K. *Electrochemistry in Nonaqueous Solutions*; Wiley, 2002.
(66) Raymond, K. N. Tragic Consequence of Acetonitrile Adduct. *Chem. Eng. News* **1983**, *61*, 4.
(67) Bastian, R.; Weberling, R.; Palilla, F. Determination of Iron by Ultraviolet Spectrophotometry. *Anal. Chem.* **1956**, *28*, 459.
(68) Gans, P.; O'Sullivan, B. GLEE, a new computer program for glass electrode calibration. *Talanta* **2000**, *51*, 33.
(69) (a) Gampp, H.; Maeder, M.; Meyer, C. J.; Zuberbühler, A. D. Calculation of Equilibrium Constants from Multiwavelength Spectroscopic Data - I. Mathematical Considerations. *Talanta* **1985**, *32*, 95. (b) Rossotti, F. J. C.; Rossotti, H. S.; Whewell, R. J. The Use of Electronic Computing Techniques in the Calculation of Stability Constants. *J. Inorg. Nucl. Chem.* **1971**, *33*, 2051. (c) Gampp, H.; Maeder, M.; Meyer, C. J.; Zuberbühler, A. D. Calculation of Equilibrium Constants from Multiwavelength Spectroscopic Data - II. Specfit: Two User-Friendly Programs in Basic and Standard Fortran. *Talanta* **1985**, *32*, 257. (d) Gampp, H.; Maeder, M.; Meyer, C. J.; Zuberbühler, A. D. Calculation of Equilibrium Constants from Multiwavelength Spectroscopic Data—IV: Model-Free Least-Squares Refinement by Use of Evolving Factor Analysis. *Talanta* **1986**, *33*, 943.
(70) Marquardt, D. W. An Algorithm for Least-Squares Estimation of Nonlinear Parameters. *J. Soc. Ind. Appl. Math.* **1963**, *11*, 431.
(71) Maeder, M.; Zuberbühler, A. D. Nonlinear Least-Squares Fitting of Multivariate Absorption Data. *Anal. Chem.* **1990**, *62*, 2220.
(72) Kolthoff, I. M. *Treatise on Analytical Chemistry. Part 1, Theory and Practice. Thermal Methods*; John Wiley & Sons, 1993.
(73) Ashnagar, A.; Bruce, J. M.; Dutton, P. L.; Prince, R. C. One- and Two-Electron Reduction of Hydroxy-1,4-Naphthoquinones and Hydroxy-9,10-Anthraquinones: The Role of Internal Hydrogen Bonding and its Bearing on the Redox Chemistry of the Anthracycline Antitumour Quinones. *Biochim. Biophys. Acta* **1984**, *801*, 351.
(74) Tsierkezos, N. G. Cyclic Voltammetric Studies of Ferrocene in Nonaqueous Solvents in the Temperature Range from 248.15 to 298.15 K. *J. Solution Chem.* **2007**, *36*, 289.
(75) Sawyer, D. T.; Sobkowiak, A.; Roberts, J. L. *Electrochemistry for Chemists*; Wiley, 1995.
(76) Bio-Logic Company. *Biokine User's Manual*, version 3.0; Bio-Logic Company: Echirolles, France, 1991.
(77) Nelder, J. A.; Mead, R. A Simplex Method for Function Minimization. *Comput. J.* **1965**, *7*, 308.
(78) Yeramian, E.; Claverie, P. Analysis of Multiexponential Functions without a Hypothesis as to the Number of Components. *Nature* **1987**, *326*, 169.

DOI: 10.1021/acsomega.8b03332
ACS Omega 2019, 4, 4871−4887